CARTOGRAPHIC POTENTIAL OF ASTER VNIR IMAGERY

by

LARRY D. LUND

(Under the Direction of C.P. Lo)

ABSTRACT

Published research papers on the Advanced Spaceborne Thermal Emission and Reflection radiometer (ASTER) have assessed either its thematic (land cover classification) or its heighting (stereoscopic terrain modeling) accuracies, with heighting assessments primarily of high-relief terrain. This thesis takes a comprehensive approach to assessing ASTER's cartographic potential by examining both thematic and heighting accuracies in an area of moderate relief. Using Level 1-B processed VNIR imagery, land cover was classified using supervised and unsupervised techniques yielding approximate overall accuracies of 76% and 83% respectively. Stereoimages of the same area were then oriented and used to locate and measure coordinates of 50 GPS points collected throughout the image area, generate a digital elevation model (DEM), and digitize contours. Comparison of these three terrain measures with reference data yielded a heighting accuracy of ±11 meters, adequate for 1:50,000 or smaller scale mapping. Significant elevation errors caused by high tree canopies were also noticed.

INDEX WORDS: ASTER, Land Cover, Classification, Satellite, Stereo, DEM, Terrain Model, Thesis, University of Georgia, Larry Lund

CARTOGRAPHIC POTENTIAL OF ASTER VNIR IMAGERY

by

LARRY D. LUND

B.A., Geography, University of Colorado, 1991

A Thesis Submitted to the Graduate Faculty of the University of Georgia in Partial Fulfillment of the Requirements for the Degree

MASTER OF SCIENCE

ATHENS, GEORGIA

2006

CARTOGRAPHIC POTENTIAL OF ASTER VNIR IMAGERY

by

LARRY D. LUND

Major Professor: C.P. Lo

Committee: E. Lynn Usery
Xiaobai Yao

Electronic Version Approved:

Maureen Grasso
Dean of the Graduate School
The University of Georgia
May 2006

Table of Contents

Page

List of Tables

Page

List of Figures

Page

Chapter 1

Introduction

Since the beginning of the space age, terrestrial mapping from orbiting satellites has undergone dramatic technological advances. Cartographic accuracies and applications unforeseen from space-based platforms as recently as the mid-1980s (Petrie, 1985, p. 140) are today being realized by a variety of nations and companies around the world. What began in the 1960s as rare opportunities for simple, hand-held frame camera photography from the cockpit of Gemini spacecraft developed, by the turn of the 21st century, into the robust, reliable, redundant, and remarkably accurate sciences of space-based digital photogrammetry and remote sensing.

The growth of satellite mapping science, and the industries it has spawned, has been accelerated by the digital computer revolution and the concomitant adoption of geographic information systems (GIS) for display, query, analysis, modeling, and forecasting of geographic phenomena (Lo & Yeung, 2002). The wide range of applications to which these products of cartographic evolution are, and will be, applied includes a variety of scientific, social, political, agricultural, military, and natural resource disciplines (Mondello, *et al,* 2004).

Primary to most of these disciplines is the base map: a cartographic product usually comprised of hypsographic, hydrographic, and other topographic features such as roads, buildings, forests, etc. relevant to basic spatial terrain and feature descriptions onto which additional, or "value-added", data are compiled (University of Texas, 2004). Mondello, *et al*

(2004, p. 51), report that the most common data application in the commercial sector of the remote sensing industry for the next several years will remain topographic base mapping and the most common method of compiling those data will be photogrammetry. Paradoxically, the need for photogrammetric professionals is also expected to decline likely due to the rapid implementation of automated digital photogrammetric techniques and airborne laser scanning, or lidar, as airborne mapping tools. The market for base map and value-added GIS data compiled from Earth imagery, both satellite and aerial. is expected to double by 2010, with satellite data comprising one third of the predicted total (p. 12). Ironically, however, the ASTER sensor, on which this paper's research concentrates, was not included among Mondello, *et al* (2004, p. 16), "primary current satellite sensors and platforms."

Such predictions for the future of remotely sensed map data could not have been reliably made if significant growth in both the number and accuracy of orbiting Earth sensors was not already underway. Due to an ever-changing geo-political landscape, which included the end of the cold war and the beginning of a global war on terror, the continued meteoric rise in computer power and storage capacity, and the ongoing myriad environmental challenges associated with land use and development, population distribution, natural resource management, and climate change, realizing the above predictions for the photogrammetric mapping industry seems likely.

Orbiting above this circumstantial substrate are a variety of new satellite sensors collecting topographic information at previously unimagined spatial resolutions, an essential ingredient to their usefulness for Earth terrain mapping. The nomenclature for these higher resolutions, like the nomenclature for many emerging and developing technologies, has never been universally consistent, and due to the concomitant rapidity of technological advancements has changed almost as often as the instruments themselves. What were once described by the

Earth mapping community in the 1970s as "high" spatial resolution sensors, e.g., the early Landsats with 79m ground pixels (Petrie, 1970), were considered less than high resolution by the 1980s with the availability of 10 m SPOT data (Dowman & Peacegood, 1989). The arrival in the late 1990s of Ikonos 2 satellite data with 1m ground pixels, followed a couple years thereafter by QuickBird II imagery with 0.6 m ground pixels, spawned another taxonomic change to the spatial resolution lexicon. The loosely defined term "high resolution" (HR) adopted during the 1980s, approximately 10 m - 30 m pixels, generally retained its meaning into the 21st century (Giri, *et al,* 2003; Comber, *et al,* 2004, Stoney, 2006), but new categories such as "very high resolution" (VHR) and "ultra high resolution" (UHR) were added to the remote sensing dictionary (Bjorgo, 2000; Kim & Muller, 2002; Ehlers, *et al,* 2003, IEEE, 2003, Chmiel, *et al*, 2004). While no explicit bounds for these categorical labels have been universally adopted, VHR, in the context of satellite mapping, now usually refers to ground pixel dimensions between 0.5 m and 9 m, while UHR usually refers to ground pixels less than 0.5 m in diameter, not yet available with declassified satellite technology but contracted for commercial production by the USDOD with GeoEye, Inc.). While these descriptive distinctions between ranges of spatial resolutions have never been universally accepted by the remote sensing community (cf. Hurtt, *et al*, 2003; Sawaya, *et al*, 2003, Chauhan, *et al*, 2003), they are assumed and used in this thesis.

Situated within the HR instrument category with a 15 m X 15 m instantaneous field of view (IFOV) is the joint Japanese-American Advanced Spaceborne Thermal Emission and Reflection radiometer, or ASTER. Like its Landsat predecessors traversing identical orbital paths, which include its Thematic Mapper (TM) contemporaries, ASTER was designed to study and monitor a wide variety of Earth surface land use/cover phenomena (Abrams & Hook, 1995). Unlike the Landsats, however, ASTER is capable of acquiring stereoscopic images in its band 3

using a backward looking telescope and along-track scanning in each orbit. The ability to stereoscopically model Earth surface terrain augments the number of remote sensing applications where ASTER can be used, making the instrument functionally competitive with several other currently orbiting HR and VHR sensors.

While ASTER data concede a technical advantage to many of these new VHR sensors in terms of spatial, and in some cases radiometric, resolution, ASTER's public ownership and management afford it a practical advantage in terms of data cost to users. Since spatial resolution is often less critical than spectral and radiometric resolution for many land use/cover analyses (Toll, 1985), and since ASTER's spectral resolution in the visible/near-infrared (VNIR) range is equivalent to, or marginally better than, its orbiting multispectral competitors (Table 1), the value of ASTER data for a variety of cartographic purposes, both thematic and topographic, should be relatively high.

Determination of ASTER's cartographic potential with respect to the satellite remote sensing/Earth mapping milieu in which it exists, therefore, is the purpose of the research conducted for this thesis. This involves (1) determining the positional and height accuracy of the data for topographic mapping, and (2) the thematic accuracy of data for the extraction of land cover information. If ASTER data can be shown to be as metrically and radiometrically accurate as they were predicted to be (Welch, *et al*, 1998), they can be a cartographically viable and economically competitive space-based remote sensing and mapping imaging option from among an ever-growing list of high- and very-high-resolution Earth-observing land cover classification/terrain mapping satellites.

Table 1.1: Active Stereoscopic Earth-Mapping Satellite/Data Characteristics. Satellite proprieties are governmental if listed by country, private if listed by company. Sensor names are abbreviated. Swath widths are not necessarily identical with scene widths. Revisit rates are not necessarily from identical nadir views. Cost values are reprinted or calculated from most recently published data (if available). Inactive stereoscopic satellite data remain available but due to the importance of image recency to surface mapping accuracy, only data from active sensors are listed. Published sensor characteristic discrepancies between official and otherwise reliable sources are not uncommon. Information presented here represents the most authoritative and/or reliable sources available (see Chapter 1 Endnotes: Table 1 Sources).

Very High Resolution

					IFOV (# Bands)							
Satellite	**Launched**	**Propriety**	**Sensor(s)**	**Swath (km)**	**Pan**	**VNIR**	**SWIR**	**TIR**	**Rad. Res.**	**Revisit**	**Stereo**	**Cost/Sq. Km**
Monitor-E	2005	Russia	PSA	90 160	8m (1)	~ 20m	~	~	Unpublished "	Unpublished "	AT/XT	Unpublished "
		(Rosaviakosmos)	RDSA		~	(3)	~	~			AT/XT	
ROCSAT-2	2004	Taiwan (NSPO)	RSI	24	2m (1)	8m (4)	~	~	Unpublished	1 day	AT / XT	Unpublished
ORBView-3	2003	Orbimage*	OHRIS	8	1m (1)	4m (4)	~	~	11 bit	3 days	AT / XT	$6 - $24
SPOT 5	2002	Public/Private	HRS	120	2.5m (1)	2.5m (3)	~	~	8 bit	3 days	AT / XT	$3.72 - $6.12
		----------	HRG	60 60	5m (1)	5m (3)	~	~	"	"	"	$1.86 - $4.26
		Owner: France (CNES)	HRG	60	10 (1)	10m (3)	~	~	"	"	"	$1.30 - $2.40
		----------	HRG	2200	~	~	20m (1)	~	"	" "	"	$1.30 - $1.86
		Operator: Spot Image	VMI		~	1150m (3)	1150m (1)	~	"		~	~
Quickbird-2	2001	DigitalGlobe	BGIS 2000	16.5	0.6m (1)	4m (4)	~	~	8 bit	3 days	AT / XT	$36 - $48
EROS A1	2000	ImageSat	PIC	12.5	1.8m (1)	~	~	~	11 bit	5 days	AT / XT	$5 - $16.46
IKONOS-2	1999	Space Imaging*	OSA	11	1m (1)	4m (4)	~	~	11 bit	3 days	AT / XT	$80 - $100
IRS-1C & 1D	1D: 1997	India (ISRO)	Pan	70	6m (1)	~	~	~	6 bit	3 days	XT	$1.08
	1C: 1995		LISS3	142	~	23.5m (3)	70.5m (1)	~	7 bit	"	~	~
			WiFS	774	~	188m (2)	~	~	"	"	~	~

* Space Imaging was purchased in early 2006 by Orbimage, which was renamed to GeoEye.

High Resolution

					IFOV (# Bands)							
Satellite	**Launched**	**Propriety**	**Sensor(s)**	**Swath (km)**	**Pan**	**VNIR**	**SWIR**	**TIR**	**Rad. Res.**	**Revisit**	**Stereo**	**Cost/Sq. Km**
IRS-P6	2003	INDIA (ISRO)	LISS-4 LISS-3 AWiFS	24 or 70 141 740	~ ~ ~	6m (3) 23.5m (3) 56m (3)	~ 23.5 (1) 56m (1)	~ ~ ~	7 bit 7 bit 8 bit	5 days 24 days 24 days	XT ~ ~	$1 - $2.80 " "
BilSat-1	2003	Turkey (BILTEN)	PANCAM	300 300	13m (1)	~	~ ~	~	8 bit	?	AT / XT	Unpublished
			MSIS		~	27m (4)		~	8 bit	?	"	"
CBERS-2	2003	China / Brazil	HRCC	113 120	20m (1)	20m (4)	~ 80m	~	8 bit	26 days "	XT	Restricted Access
		(CAST)/(IPE)	IRMSS		80m (1)	~	(2)	160m (1)	8 bit		~	
TERRA	1999	US / Japan (NASA / MITI)	**ASTER**	60	~	15m (3)	30m (6)	90m (5)	8 bit	16 days	AT / XT	**$0.05**
SPOT 4	1998	Owner: France (CNES)	HRV	60	10m (1)	20m (4)	~	~	8 bit	3days "	XT	$1.30 - $6.12
		Operator: Spot Image	VMI	2200	~	1150m (4)	~	~	8 bit		~	~

Chapter 1 End Notes**:**

Table 1.1 Sources: Web sites visited in September, 2004 and March, 2006

http://www.spotimage.fr/automne_modules_files/standard/public/p336_fileLINKEDFILE_Price_List_2004.pdf
http://www.digitalglobe.com/downloads/QuickBird%20Imagery%20Products%20-%20Price%20Table.pdf
http://carstad.gsfc.nasa.gov/topics/JBRESEARCH/HSSRProject.htm#bilsat
http://directory.eoportal.org/pres_MonitorEMonitorExperimental.html
http://www.imagesatintl.com/productsservices/pricingguide.shtml
http://www.gisdevelopment.net/aars/acrs/2000/ps1/ps113.shtml
http://flash.lakeheadu.ca/~bmwelmer/remote_sensing/IRS.htm
http://directory.eoportal.org/res_p1_Operationalmission.html
http://geo.arc.nasa.gov/sge/health/sensor/cfsensor.html
http://www.geoserve.nl/pricelists/pricelist_SIEA.pdf
http://directory.eoportal.org/pres_DMCmission.html
http://aria.seas.wustl.edu/SSC02/papers/viii-3.pdf
http://www.cbers.inpe.br/en/imprensa/not1.htm
http://www.orbimage.com/partn/Terraserver.htm
http://www.intecamericas.com/IRS.htm
http://www.tbs-satellite.com/tse/online/
http://www.isro.org/pslvc5/index.html
http://www.gstdubai.com/pricelist.htm
http://www.astronautix.com/craft/

Chapter 2

Status of Topographic Mapping from Space

Typical of most topographic maps, whether the source survey was space-based or otherwise, are planimetry and hypsography (Maune, *et al,* 2001). A wide variety of surface features, unique to the intended purposes defining each topographic project, comprise the various types of planimetry. Planimetric features are usually classified as natural (e.g. hydrography, vegetation) or man-made (e.g. roads, buildings) and collectively comprise the elements of respective thematic feature classes depicted cartographically. Hypsography, the depiction of continuous surface elevations (usually with vectorized contours or shaded raster arrays), usually includes discrete spot elevation measurements, made at clearly identifiable locations in both the source data and the finished map, which are held to a higher standard of accuracy than the continuous surface being represented (NMAS, 1947). While other national (including western European) standards for spot height accuracy often exceed US standards, the same accuracy relationship between spots and contours exists.

As this chapter will explore, the techniques and methods employed in the capture, storage, processing, and display of photogrammetric data have radically changed since the transfer of imaging technology from aerial to orbital platforms began at the inception of the space age in the mid-20th century. Concomitant with these technological advances have been dramatic increases in the demand for terrain model and LU/LC datasets as the need for environmental monitoring of resources, pollution, development, and climate have become

increasingly evident (though the constant shifting of political winds does not guarantee such a need will always be evident) . What have not changed in the face of these changes are the accuracy standards to which cartographic products are held. Reaching for, then maintaining, those standards has produced the plethora of carto-capable satellites in orbit today.

The evolution of satellite photogrammetric techniques paralleled, to a great extent, the evolution of aerial photogrammetric techniques, the primary difference being one of altitudinal degree. As with much of science during the second half of the 20th century, the application of automated and computerized technology to previously manual and analog processes radically increased the volume of processes that could be completed. The advent of automated triangulation algorithms for ground-to-image and image-to-image conjugate point coordinate calculations made possible in the 1970s by programmable "mini" computers vastly reduced the formerly manual computation times for photogrammetric image orientations.

The arrival in the 1980s of analytical stereoplotting instruments with computer-controlled, servo motor-driven image tracking systems greatly reduced stereopair orientation times on previously state-of-the-art analog stereoplotting instruments. Advances in optical physics, lens design, and photographic film chemistry accompanied the transition from analog to analytical stereoplotting, thereby increasing photogrammetric accuracies from higher platform altitudes, including orbital altitudes.

The 1990s, with its exponential growth in digital technologies, witnessed several revolutions in photogrammetric techniques. The collection of ground control points, to which aerial imagery is registered, a process known as absolute orientation, became GPS-, rather than theodolite-, based. Global Positioning System (GPS) receivers were also added to aerial survey aircraft as part of integrated Inertial Navigation Systems (INS), rendering rapid-interval, usually

on the order of one second, positional data for the on-board cameras. Exposure epochs occurring between GPS intervals are interpolated from computer-modeled aircraft trajectories generated from the INS data. This technique, known as Airborne GPS (AGPS), greatly reduced the required ground control network point density from several points every few images in each overlapping flight line to several points in an entire project area. Analog, film-based photographic images could also be optically scanned at micron-scale resolutions into digital raster files spatially addressed by pixel number rather than by distance from an image reference frame origin. As computer processors became increasingly more powerful and computer memory and disk space became increasingly more available, digital management of the volume of information that accompanies the manipulation of paired, oriented raster files, as well as the superimposed, user-generated vector files, i.e. operator-compiled cartographic data, that photogrammetry enables, became a reality. That reality of replacing hardcopy imagery in the photogrammetric workflow was called, not surprisingly, softcopy photogrammetry.

The turn of the 21st century brought with it yet another turn in the technical pathway of photogrammetric techniques. Large-scale mapping projects with precision accuracies, which were too costly for most organizations to afford for large areal coverages during the analog photogrammetry age, became the rule rather than the exception due to technological advancements. Those advancements economized the development of large-format digital aerial cameras employing Charge-Coupled Device (CCD) arrays capable of capturing images at or very near the spatial resolution of conventional film-based cameras. The entire photogrammetric process, therefore, had become a closed digital loop, with each step in that process aided, if not completely defined, by high-speed, computerized, solid-state circuitry.

The first non-military stereoscopic photographs taken from space were captured with hand-held cameras during NASA's Gemini missions in the 1960s, but the few image pairs acquired realized little in the way of application or accuracy. The first non-military attempts at satellite photogrammetry were made several years later, but not with Earth as the photographic object. Instead, imagery captured aboard the Apollo 15, 16, and 17 missions to the moon during the late 1960s and early 1970s comprised the first serious space-based photogrammetric experiments, eventually resulting in 1:25,000 scale topographic orthophotos or scale-corrected image maps of the moon (Doyle, 1979).

With the launch of NASA's Skylab mission in 1973, photogrammetric Earth mapping from satellites became a directed, albeit experimental, reality. The Earth Terrain Camera (ETC) onboard SkyLab in 1974 produced the first along-track stereo images of Earth, i.e. imaging directly below, rather than adjacent to, each orbital path, taken from space were capable of measuring terrain elevations (Mott, 1975) but the 120m vertical accuracies as measured by the vertical root mean square error (RMSEz) allowed for a minimum contour interval of only 250m. The ETC images, therefore, were useful only in areas of very high relative relief.

Various East German, Russian, and European Space Agency-sponsored efforts at space-based Earth photography followed during the 1970s and early 80s, but due to various systematic problems including areal discontinuities, lack of forward motion compensation (FMC), and non-stereoscopic and/or low base to height ratio (B/H) imagery, no useful photogrammetric applications were realized (Toutin, 2001a).

During the 1980s, NASA's FMC-capable Large Format Camera (LFC) was twice deployed aboard the Space Shuttle conducting a plethora of analytical photogrammetric experiments yielding positional and altimetric RMSEs adequate for most 1:50,000 scale mapping

(Gruen and Speiss, 1986; Togliatti and Morionodo, 1986; Murai, 1986; Buchroithner et al, 1987). Several years later, LFC imagery was also tested for thematic mapping potential using the USGS-Anderson land use/cover classification scheme (Anderson, *et a*l, 1976), which contains the hypothetical and parametric bounds for the thematic portion of the research goals and methods used for this thesis. Accuracy standards were not met by LFC for detailed Anderson Level III classifications but accuracies were observed to be marginally lower than those obtained using National High Altitude Photography (NHAP) imagery and were suitable for some Level II classifications. Such thematic accuracies are also typical of 1:50,000 scale mapping (Lo & Noble, 1990).

While not designed for stereoscopic applications, NASA's Landsat Multispectral Scanners (Landsats 1-7) and Thematic Mappers (Landsats 4-7) have been examined for their stereoscopic terrain mapping potential (Welch & Lo, 1977; Simard, 1983; Welch & Usery, 1984; Simard and Slaney, 1986). The reliability of digital elevation models (DEMs) generated from stereocorrelation in those studies was statistically dubious, though, at least by today's standards, due to the unavailability of reference DEMs to compare with those results (Toutin, 2002b). The technical difficulties of orienting and evaluating Landsat stereopairs, e.g. degraded image quality and problematic pixel correlations due to temporal mismatches (i.e. seasonal land cover differences, variable atmospheric conditions, different solar-to-sensor angles, etc.), also characterized Landsat stereo research. These challenges notwithstanding, hypsographic accuracies with Landsat sensors have been achieved for scales ranging between 1:100,000 and 1:250,000 (Simard and Krishna, 1983; Ehlers & Welch, 1987; Toutin, 2002b).

The thematic land use/cover classification potentials and accuracies of the various Landsat sensors has been widely researched, published, and applied over their thirty-plus years

of existence. Classification methods have evolved from early supervised (i.e. manually trained)) and unsupervised, i.e. semi-automated, algorithms (Hord & Brooner, 1976; Odenyo & Pettry, 1977) to a variety of advanced applications in the interpretation of fractal patterns (De Cola, 1989), the use of fuzzy logic (Wang, 1990), artificial intelligence (Moller-Jensen, 1990; Wilson, 1997), neural networks (Bischof, *et al*, 1992), and new hybrid classification techniques (Lo & Choi, 2004; Liu, *et al*, 2004). Methods of assessing the accuracies of these techniques have likewise evolved from simple error matrix-based approaches (Van Genderen & Lock, 1977) to include multivariate and spatially autocorrelated statistical methods (Congalton, *et al*, 1983, Congalton, 1988) with an additional Tau correlation coefficient appending the original Kappa (Ma & Redmond, 1995).

With the launch of the first French SPOT-HRV satellite in 1986 a new era of space-based land cover/stereoscopic terrain mapping began. SPOT-1's 10m panchromatic and 20m IFOVs, were achieved with "pushbroom" scanner technology rather than an analog frame camera such as the LFC or an oscillating optical-mechanical "whiskbroom" scanner such as those aboard the Landsats. This linear array of solid state, charge-coupled devices (CCDs) would become the scientific standard in virtually all Earth observing satellites (excepting the Landsat and Sino-Brazilian CBERS series) because it closed the digital loop, i.e. data would not require terrestrial analog-to-digital conversion, had better geometry, and improved IFOV stare duration, effectively increasing the volume of radiant energy incident upon the CCDs (Jensen, 2000). The SPOT instrument also employed a pointable telescope providing cross-track stereoscopic imaging, i.e. one of the two telescopes looks sideways into an adjacent orbital path. SPOT was, therefore, the first Earth observing satellite specifically designed to enable stereoscopic terrain modeling from

space. Those accuracies were verified to be adequate for 1:25:000 to 1:50,000 scale mapping with 5m-10m RMSEz (Gugan and Dowman, 1988; Dowman, 1994).

The end of the cold war brought several new competitors to the mapping-from-space race. Beginning with declassified Russian space photography captured with the KFA, KVR, and TK series cameras aboard Resurs F-1 and F-2 and Komet satellites respectively, accuracies adequate for 1:25,000 scale topographic mapping were achievable with film photography from 100cm focal length analog frame cameras (Muller, et al, 1994; Kaczynski, 1995; Jacobsen, 1998; Büyüksalih, *et al*, 2003). The availability in the early 1990s of Russian VHR space photography led the US Department of Defense to declassify US VHR satellite technology, opening the economic door for private satellite companies in the US to begin launching VHR sensors before the end of the 20th century.

During the 1990s, a variety of HR topographic mapping sensors would be built around the world. The Japanese Earth Resources Satellite (JERS-1) was launched in 1992 followed by their Advanced Visible and Near Infrared Radiometer (AVNIR) in 1996. The Indian Remote Sensing satellites (IRS 1C & 1D) were launched in 1995 & 1997, respectively. Germany's Modular Optoelectronic Multispectral Scanner (MOMS-02) flew one 10-day mission aboard the Space Shuttle (STS-55, 1993) and another 18-month mission aboard the Russian Mir space station (1996-98). Cartographic accuracies adequate for mapping at 1:25,000 to 1:50:000 scales had become typical with these instruments, achieving 5 m-15 m RMSEz (Konecny & Schiewe, 1996). The seventh, and possibly final, installment to the US Landsat program (Mondello, *et al*, 2004), the Enhanced Thematic Mapper Plus (ETM+), was launched in 1999 but its non-stereoscopic 30m multispectral imaging technology was designed for thematic mapping (augmented by a new 15 m panchromatic sensor) rather than terrain modeling applications.

What began the 1990s with the declassification of Russian space photography ended the 20th century with a VHR satellite image revolution. The successful launch of Ikonos 2 in 1999 by Space Imaging, Inc. also ushered in the age of privately financed and owned mapping satellites. The successful launch and implementation of the Israeli EROS A1 satellite in 2000 (by ImageSat International), QuickBird 2 in 2001 by DigitalGlobe, Inc., SPOT-5 in 2002 (the SPOT series, while privately managed, is publicly funded), Orbview-3 in 2003 by Orbimage, Inc., ROCSAT 2 in 2004 by Taiwan, and Monitor-E (by the ISC, or Russia) in 2005 brings to eight the number of active stereoscopic satellites in the VHR constellation (Table 1). Not surprisingly, several others are also planned and/or under construction (Sandau, 2003, Jacobsen, 2005, Stoney, 2006). All seven orbiting sensor systems offer both along-track and cross-track stereo imaging and each is capable of cartographic accuracies compatible with 1:25,000-or-greater scale mapping (Ridley, *et al*, 1997; Shi & Shaker, 2003; Tolono & Poli, 2003; Büyüksalih & Jacobsen, 2004; Noguchi, *et al*, 2004; Mulawa, 2004; Toutin, 2004a; as of this writing there are no published data on the cartographic accuracies of Monitor-E). Three of the five sensors, Ikonos 2, QuickBird 2, and Orbview-3, capture 1m-or-less IFOV data from orbits several hundred kilometers high (EROS A1's ground pixel dimension is just under 2m). While SPOT-5 captures standard panchromatic color imagery with a 5m IFOV, additional user cost (up to $7,500 per 3600 km^2 scene; CNES 2003a) delivers combined, contemporaneously captured images from identical onboard sensors at 2.5m IFOV (CNES, 2003b).

The ASTER sensor, to be discussed in more detail below, was launched in late 1999 shortly after the IKONOS 2 satellite as a sensor onboard NASA's Terra satellite. Without a panchromatic sensor and only a 15m multispectral IFOV for its VNIR bands, ASTER is not a true VHR sensor. However, with twice the multispectral spatial resolution of the Landsat

Thematic Mapper which it was designed to augment or replace (Welch, *et al*, 1998; *cf.* Fig. 3.2 below) and its superb visible and near-infrared (VNIR) sensor geometry, optics, and radiometric resolution (Büyüksalih & Jacobsen, 2004), ASTER has often been descriptively (if not categorically) included with orbiting VHR sensors in the space-based photogrammetric literature (Toutin, 2001a; Aniello, 2003; Büyüksalih & Jacobsen, 2004; Ma, 2004). This hybridized approach to sensor design, ostensibly capable of extracting VHR-accuracy terrain spot heights with larger-than-VHR image footprints and IFOVs, is unique to ASTER. In fact, Aniello (2003) reports that ASTER DEMs constitute adequate surface model substrates for most IKONOS image orthorectifications. Combined with the public ownership of ASTER via NASA and METI (Japan's Ministry of Economy, Trade, and Industry), which subsidize data costs and hence their effective availability to users, the worthiness of ASTER as a subject for the research attention paid to it, both in this thesis and elsewhere, should be evident.

While not the primary focus of this thesis, there are both viable, albeit expensive, and non-viable alternatives to stereoscopy for satellite-based digital terrain modeling and a brief mention of them will be made here. First, space-based radar mapping is an increasingly popular terrain modeling technique. Currently, however, most of the available global radar datasets are expensive to acquire, such as Canada's RADARSAT-1 and -2 (at least relative to ASTER DEMs). Besides being generated by sensors that are relatively expensive to build, the relative cost of space-based radar data reflects the higher demand for their generally higher level of accuracy. Light Detection and Ranging (LiDAR), or laser distance scanning, while gaining significant use and support as an airborne terrain modeling technique for larger map scales, has not been widely pursued by space-based Earth mapping interests due to the reduced altimetric posting densities achievable from orbital elevations (Toth, *et al*, 2001). Clinometry, i.e. image

shading and shadowing analysis, provides reliable heighting measurements of bare earth surfaces (Cheng and Thiel, 1995), but only in relative contexts absent comparisons to existing digital terrain data.

Because of these financial and technological constraints associated with competing space-based terrain modeling technologies, generating DEMs for moderate to large Earth surface areas (*e.g.* between the areal extents of cities and states) can often be accomplished quickly and economically using satellite stereoscopy. It is for that growing market that private remote sensing technology companies and a variety of national governments around the world have begun developing orbiting systems to meet the demand. Evaluating ASTER's potential within that academic, scientific, and market-driven milieu was the purpose of this project.

Chapter 3

The ASTER Sensor

Sensor Characteristics

The ASTER sensor flies aboard NASA's flagship Earth Observing System (EOS) satellite called Terra (formerly EOS AM-I). Launched from California's Vandenberg Air Force Base on December 18, 1999, ASTER has been operational from an altitude of 705km since March of 2000 (Hirano, *et al*, 2003) and is expected to remain operational through 2006 (Welch, *et al*, 1998).

Terra supports five separate remote sensing instruments, ASTER, Clouds and the Earth's Radiant Energy System (CERES), Multi-angle Imaging Spectro-Radiometer (MISR), MODerate-resolution Imaging Spectroradiometer (MODIS), and Measurement Of Pollution In The Troposphere (MOPITT). Each sensor aboard the Terra platform is designed with different research and observational goals in mind (Kaufman *et al,* 1998).

Spectrally, ASTER captures atmospherically transparent wavelengths from the visible and near-infrared (VNIR), short wave infrared (SWIR), and thermal infrared (TIR) regions of the electromagnetic spectrum with three separate instruments collecting data over 14 spectral bands; one of which, NIR Band 3, is recaptured stereoscopically with a pointable backward- and/or side-looking telescope. The near and short wave IR sensors record passive, or reflected, solar energy while the thermal sensor records absorbed and re-emitted solar energy. The VNIR sensor

scans with an IFOV of 15m, the SWIR sensor scans with a 60m IFOV, and the TIR sensor scans with a 90m IFOV. Table 2 describes ASTER's spectral, spatial, and radiometric characteristics.

Table 3.1: Spectral, Spatial, and Radiometric Resolutions of ASTER (Adapted from Abrams, *et al*, v. 2).

Telescope	Band #	Wavelength (µm)	IFOV	Radiometric Res.
VNIR	1	0.52 - 0.60	15mX15m	8 bit
"	2	0.63 - 0.69	"	"
"	3N	0.78 - 0.86	"	"
"	3B	0.78 - 0.86	"	"
SWIR	4	1.60 - 1.70	30mX30m	"
"	5	2.145 - 2.185	"	"
"	6	2.185 - 2.225	"	"
"	7	2.235 - 2.285	"	"
"	8	2.295 - 2.365	"	"
"	9	2.360 - 2.430	"	"
NIR	10	8.125 - 8.475	90mX90m	12 bit
"	11	8.475 - 8.825	"	"
"	12	8.925 - 9.275	"	"
"	13	10.25 - 10.95	"	"
"	14	10.95 - 11.65	"	"

The ASTER VNIR sensor represents NASA's first HR multispectral radiometer utilizing the now industry-standard digital line scan, or "push broom", technology. In the case of the VNIR sensor employed for this study, four thousand CCDs arranged in a single linear array scan individual 15m X 60km swaths of Earth's surface every few milliseconds. Following each 60km swath, the sensor immediately re-sets along an adjacent ground swath and a new image pixel row from the ground is scanned (Abrams, *et al*, v. 2).

Stereoscopic imaging is accomplished with along-track scanning when ASTER is directly above a swath 370 kilometers down range from the final swath recorded in the previous image by the nadir-looking sensor (see Fig. 3.1 below). The aft-looking sensor recording Band 3B (*cf.* Table 3.1) begins its scan of the previously nadir-scanned surface area from an oblique angle of 27.6˚ sixty seconds after the nadir-looking image is completely captured, providing a near real-

time stereo pair image match (Kääb, *et al*, 2002), something across-track stereoscopy cannot produce.

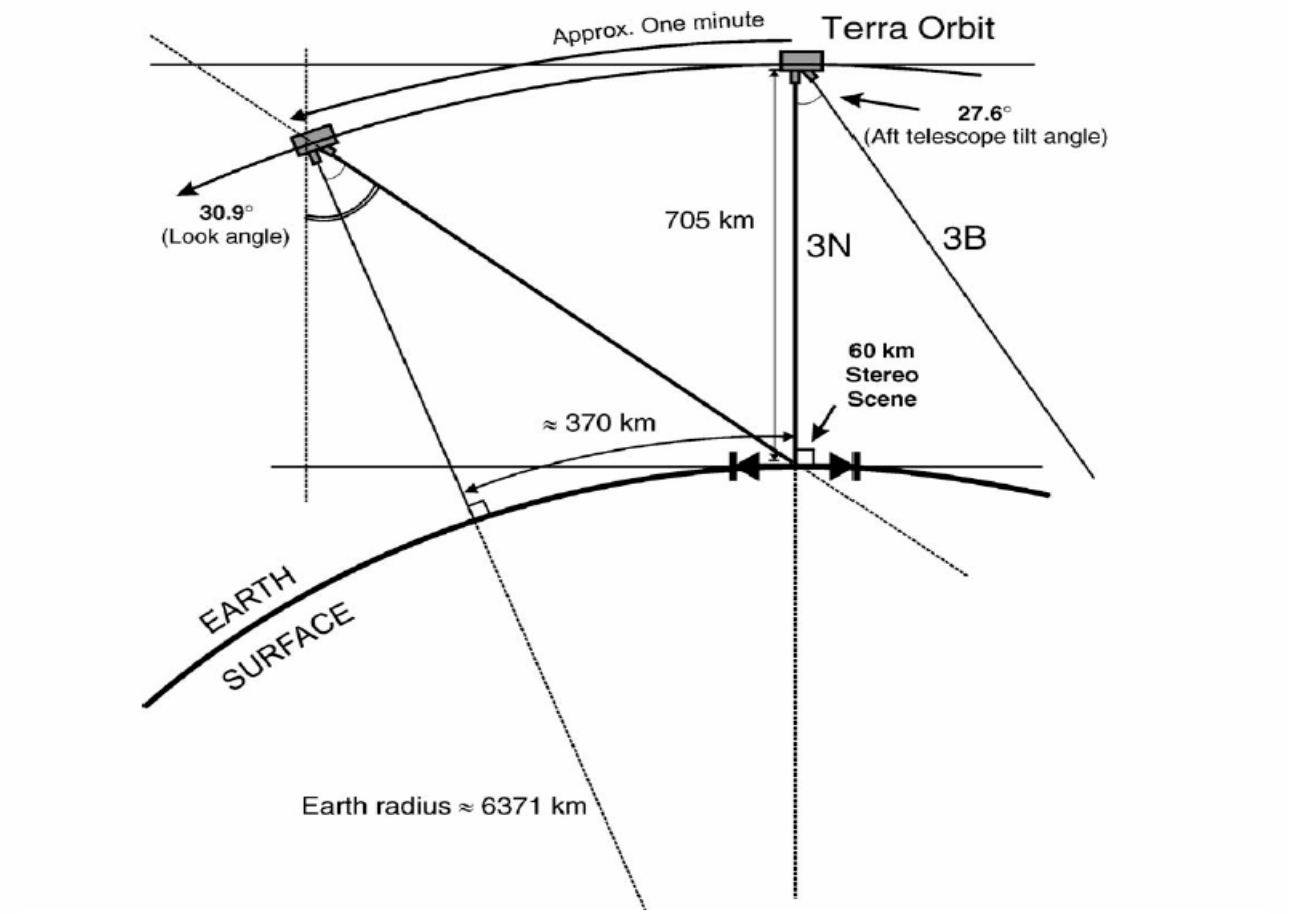

Figure 3.1: ASTER's Stereoscopic Architecture Aboard NASA's TERRA Satellite. From Hirano, *et al*, 2003.

Across-track stereoscopy, while available with ASTER data, as it is with most of ASTER's orbiting competitors such as IKONOS 2, QuickBird II, OrbView-3, and SPOT-5, is more problematic to apply due to temporally mismatched images and more complex photogrammetric orientations yielding technical hurdles to overcome such as variable base/height ratios (B/H) and application constraints to keep in mind such as spatially reduced

paired-image footprints. Along-track stereoscopy preserves spectrally and temporally matched imagery, standardized relative orientations, and a consistent B/H of 0.6, considered by many photogrammetrists to provide nearly ideal stereo exaggeration for manual elevation measurements in the broadest range of terrain variability (Hirano, *et al,* 2003). It is acknowledged, however, that a higher B/H often produces a lower RMSEz (Petrie, 1985, Welch, 1989). The nadir revisit rate for ASTER (i.e. the time between identical vertical image capture locations) is 16 days (Abrams, *et al.*, v. 2).

In addition to its stereoscopic terrain modeling capabilities, ASTER is equipped as a multi-band spectroradiometer for a variety of classical thematic remote sensing applications such as land use/cover analysis (Zhu & Blumberg, 2002), mineral mapping (Rowan & Mars, 2003), change detection (Yamaguchi, *et al*, 2001), and volcano (Yamaguchi, *et al*, 2001), fire (Wessels, *et al*, 2002), and glacier monitoring (Kääb, *et al*, 2002). Since ASTER was designed to augment or replace the Landsat series, a spectral comparison between the Landsat 7's Enhanced Thematic Mapper Plus (ETM+) and ASTER is provided in Figure 3.2.

Data Characteristics

Raw data downloaded from ASTER are reconstructed at METI's Ground Data System (GDS) office in Tokyo. Data are then transferred to the United States Geological Survey's (USGS) National Center for Earth Resource Observation & Science Data Center (EROS) for archiving, user-requested processing, and delivery from the Land Processes Distributed Active Archive Center (LPDAAC). A variety of data processing levels are available as either Standard or On-Demand products. Standard products, or those produced as standard procedure for all

archived images, include Level 1A (unprocessed), Level 1B (registered), Level 2 SDS (systematic decorrelation stretched), and Level 3 DEM datasets. Several other Level 2 processes germane to thermal remote sensing applications vis-à-vis surface temperature (brightness or

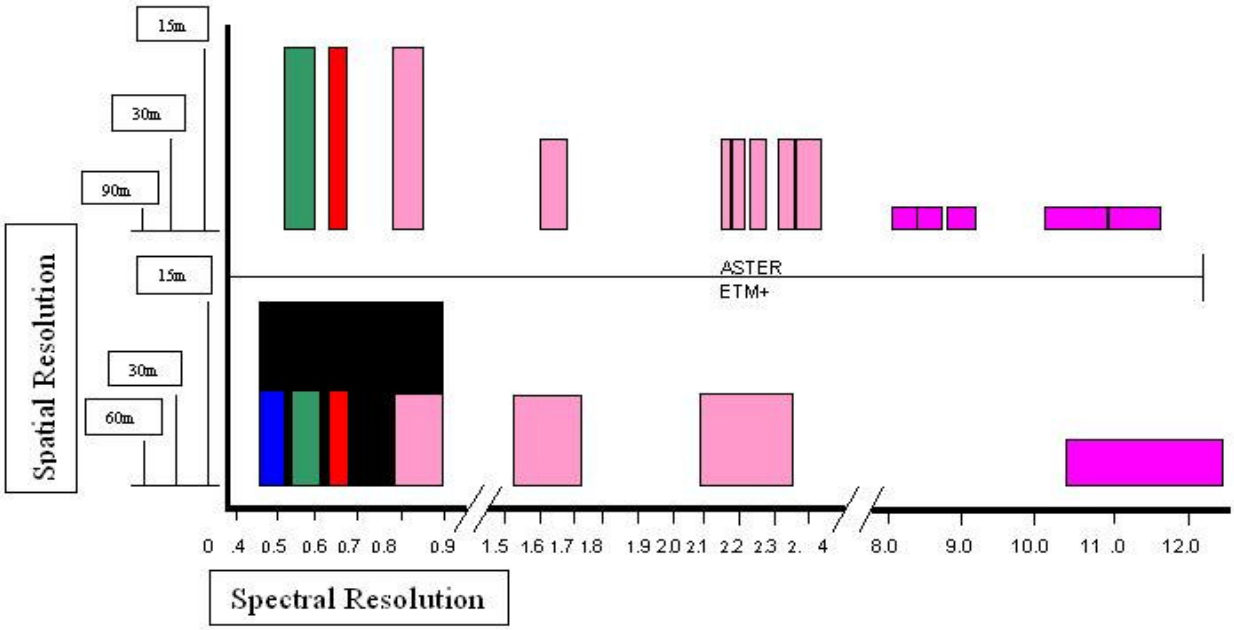

Figure 3.2: Spectral Comparison of ASTER and ETM+ (Landsat 7, Enhanced Thematic Mapper Plus). Black area denotes the 15m IFOV panchromatic sensor aboard ETM+, not included on ASTER.

kinetic), emissivity, reflectance, and radiance can be ordered in, and applied to, ASTER datasets as well. These on-demand products, excepting DEMs, employ user-specified processing algorithms applied primarily with 2D remote sensing rather than 3D photogrammetry.

Level 1A data are time referenced and annotated but the scene registration information (i.e. the radiometric and geometric calibration coefficients and the georeferencing parameters) is merely computed and appended to the metadata, not applied to the datasets themselves. Level 1B data have the calibration coefficients and georeferencing parameters applied to the datasets as

registered sensor radiance values. Level 3 data are epipolarized, stereocorrelated DEMs produced from Level 1A data, similar to the DEM produced during this research.

All datasets are delivered in Hierarchical Data Format used by sensors in the Earth Observing System constellation (HDF-EOS). Levels 1B, 2, and 3 data are projected into relevant Universal Transverse Mercator (UTM) coordinate system zones using the 1984 World Geodetic Survey reference ellipsoid (WGS-84) and are either downloadable over the Internet using file transfer protocol (FTP) or delivered on a medium of choice (USGS, 2005).

Previous Research Using ASTER Data

Surprisingly, the volume of published research evaluating ASTER VNIR data for land cover classification is quite small considering its duration of operation, now nearing the end of its expected 6-year mission. The research conducted on ASTER's terrain modeling capacity, however, is relatively abundant, though much of that research has been presented at various mapping symposia around the world and/or published on the World Wide Web in addition to the mainstream remote sensing journals during the last few years. A more detailed discussion of the published and presented topographic and thematic results from ASTER data is warranted here.

Prior to ASTER's launch, Welch *et al* (1998) evaluated the sensor's designed capabilities by proxy, using SPOT-1 panchromatic 10m imagery resampled prior to evaluation to 15 m. The selected stereopaired imagery was captured along-track with a B/H of 0.7, providing a close simulation to ASTER's expected performance. While not utilizing ASTER data for their study (since TERRA had not yet been launched), they did use DMS software for the research. A sub-pixel stereo correlation error was achieved with one of the two examined datasets yielding an $RMSE_z$ of ± 13.5m (the other dataset, utilizing fewer control points, was slightly less accurate).

Shortly after ASTER's launch, the sensor systems were activated and a months-long process of sensor calibration and testing was begun. On February 28, 2000 the sensors recorded their first images and by mid summer of that year that the sensors were all operating at or above expected nominal levels and over 26,000 scenes had been captured.(Yamaguchi, *et al*, 2001).

Within a year of that report, Zhou & Blumberg (2002) published results using an artificial intelligence-based classification algorithm they had developed called a support vector machine (SVM) to classify urban land cover types. Overall classification accuracies were reported just below 90 percent for two urban areas of interest (AOIs) in an arid, low-vegetation area of Israel. One AOI utilized 15m VNIR data and the other used 30m SWIR data. Overall results for a non-urban, open space classification with the same two datasets were just under 95 percent.

Rowan and Mars (2003) published the first study of ASTER's lithologic classification capabilities, but those capabilities were assumed, rather than evaluated statistically, to be adequate for their tasks, i.e. no error matrices, percent correctly classified values, or specialized correlation coefficients were reported. That same year, Kamp *et al* (2002) reported on ASTER DEMs' ability to identify geomorphologic structures but, like Rowan and Mars' lithologic classification, Kamp, *et al*, did not include any statistical analysis of DEM accuracy.

Four papers have been published reporting ASTER's topographic DEM accuracy measured on glacial landforms (Kääb, *et al*; 2002, Cheng, *et al*, 2003; Vignon, *et al*, 2003, Bolch, 2004). Cheng *et al* (2003) reported DEM accuracies but only in graphical form, omitting tabular, statistical conclusions. Bolch (2004) reported $RMSE_{x-y}$ from stereocorrelation, as well as his use of SRTM data to fill cloud-caused artifacts, but no $RMSE_z$ for DEM was included. Kääb *et al* (2002) and Vignon *et al* (2003) reported several specific types of surface modeling failures by ASTER (and some potentially useful possibilities) as well as the statistical ($RMSE_z$) values

germane to topographic accuracy assessment. Those $RMSE_z$s ranged from 18 m to 60 m depending on terrain type. Vignon *et al* (2003) cited steep terrain aspects relative to sensor look angles as being particularly problematic (some of the so-called back slopes were left unprocessed in the resulting DEMs due to unmatchable pixels) while Kääb *et al* (2003) measured maximum individual elevation discrepancies ($D_z$maxes) between reference and ASTER DEMs as high as 95m in areas of abrupt, significant terrain relief. The latter team also compared reference and ASTER-generated contours, albeit only graphically, something no longer often included in topographic assessments.

Several direct comparisons between ASTER DEMs and those generated from its orbiting, Earth-observing competitors have been presented in the last few years as well. While Ma (2004) did not examine DEMs, she did compare the sensor models, data processing procedures, and georeferencing accuracies of ASTER to SPOT 5; citing, as Welch *et al* (1998) did with regards to SPOT 1, the many similarities between the two sensors. She concluded that ASTER Level 1A data were insufficiently corrected for CCD lattice vectors and instrument ephemeris to be useful for cartographic purposes.

Comparisons between spaceborne satellite DEMs have recently begun including radar-based DEMs in the studies. Ironically, the most significant similarity between these studies is the difference in their results. Some research concludes that SRTM DEMs are reliable enough to use as reference data for ASTER evaluations while other research concludes ASTER DEMs are more accurate than SRTM DEMs. Jacobsen (2003) compared twelve different orbiting sensors and cameras for DEM production including KFA-1000, MK4, KATE-200, TK-350, CORONA, SPOT 1-5, MOMS-02, IRS-1C/1D, ASTER, IKONOS 1, QuickBird, and SRTM, but does not report a consistent list of statistical conclusions regarding DEM accuracies from the study. Two

years later, however, Büyüksalih & Jacobsen (2004) report a comprehensive statistical comparison between four of those sensors (TK350, SPOT 5, ASTER, and SRTM). SPOT 5 data were cited by this study as the most accurate for DEM production, though the differences in overall $RMSE_z$s between SPOT 5 and SRTM were very small. The same results were published in another paper that same year (Jacobsen, 2005) which included a graphical comparison of contours generated from the respective DEMs.

Subramanian (2003) reported some very different conclusions. In this study, which reported linear and circular errors rather than $RMSE_z$s, an ASTER-derived DEM displayed the lowest combined errors while SPOT came in a close second. The paper did not specify which SPOT satellite supplied the data, though it is likely SPOT 5 was implied, and Radarsat rather than SRTM data were compared in the study.

GISDevelopment.net, a Web-based library of otherwise unpublished remote sensing, mapping, and GIS research, includes a study by Trisakti & Carolita (2006) comparing an ASTER DEM with an SRTM DEM in which SRTM's accuracy is assumed and qualified as reference data (a conclusion supported on a global scale by the recent report from Rodriguez, *et al*, 2006). Unlike any of the previous studies mentioned, Trisakti & Carolita compared ASTER and SRTM DEMs over the identical study area covered with heavy tree canopies and other dense vegetation on occasionally steep, mountainous slopes, conditions that affect accuracies of both sensors. Like Subramanian (2004), Trisakti & Carolita did not report an $RMSE_z$, but they did report a minimum elevation from each sensor (the study area in Indonesia included sea level terrain where the ASTER DEM recorded elevations 12 m below mean sea level), a maximum elevation from each sensor (ASTER's Z_{max} was 35 m higher than SRTM's), a mean elevation (ASTER's was 8m lower than SRTM's), a mean error of -8.6 m, and a mean absolute error of 27 m.

` The same stereoscopic dataset analyzed for this project was re-evaluated by Dr. Thomas Jordan of the Center for Remote Sensing and Mapping Sciences (UGA Dept. of Geography). Similar results to those discussed below were obtained and were co-presented with this author at the annual convention of the American Society for Photogrammetry and Remote Sensing (Jordan, *et al*, 2005).

Perhaps the most comprehensive study of ASTER's topographic capabilities, evaluating four separate datasets (although for relatively small sub-areas from each scene rather than entire or majority image areas) was published by Hirano, *et al*, in 2003. While not a comparative study between ASTER and other orbiting sensors, it did assess DEM generation capabilities in a variety of environmental settings, each with different quantities and types of control and reference data, using two different commercial off-the-shelf (COTS) stereocorrelation/DEM production software packages, including DMS used for this research. Source and reference DEMs were compared along transects, or profile lines (one per dataset), chosen for their terrain and land cover variabilities yielding $RMSE_z$s for the four areas between ±7 m and ±15 m.

Chapter 4

Research Design and Methodology

Characteristics of the ASTER Data Used

The dataset used for this research was processed to Level 1B, delivered on CD-ROM, and included all three of ASTER's bandwidths (VNIR, NIR, & SWIR, *cf.* Table 3.1). Since only the VNIR data would be analyzed for this thesis, the VNIR wavelengths were extracted from the original dataset.

The ASTER scene used for this study was captured during virtually 100 percent cloud-free conditions over northeast Georgia at 4:48 pm on September 28, 2000 (Figure 4.1). Local vegetation conditions at the time of image capture were nominal for early autumn in north Georgia. Leaf-on conditions prevailed for deciduous trees, brush, and vegetative ground cover, unlike at more northern latitudes during the same annual epoch when trees have begun to senesce and exfoliate. Heavy forest canopies, therefore, obscured ground surface views over extensive image areas. Because of this leaf-on condition, the first-surface reflected energy signatures recorded by ASTER from forest canopies covered significant portions, greater than 20 percent, of the scene. Where tree tops exceeded 30 m above ground level, common in the scene area, first-surface reflectance signatures from which the stereo images were created recorded non-terrain surfaces. i.e. canopy crowns, rather than ground. This 30 m vertical difference between

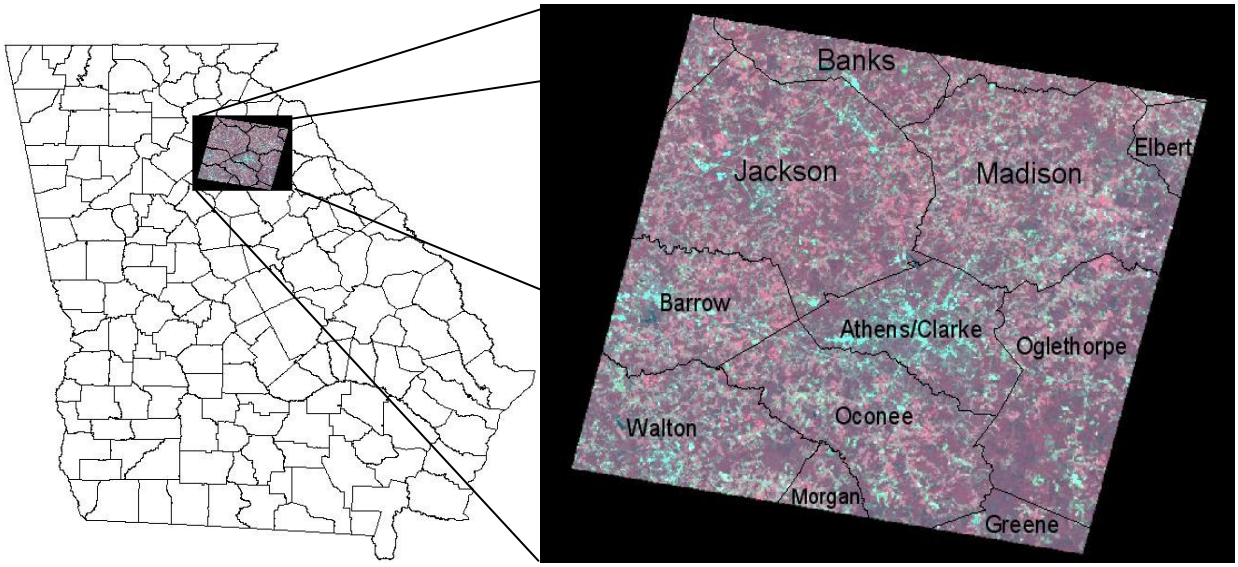

Figure 4.1: September 28, 2000 ASTER VNIR Scene. Left image: ASTER scene projected over coincident Georgia counties with ArcView. Right image: Counties are labeled. Red shades = forest, pink shades = agriculture, light blue shades = urban/developed, grey shades = soil & fallow cropland, black shades (non-background) = water.

ground elevations and stereoscopic signature measurement at the convergence of X-parallax on tree canopy crowns was equivalent to 2 or 3 times the previously reported error budget of ASTER's stereoscopy (Hirano, *et al*, 2003). X parallax is defined in digital photogrammetry as the convergence of conjugate image pixels from stereopaired images along epipolar lines enabling the interpretation and measurement of elevations. This first-surface signature phenomenon limits a wide range of photogrammetric surface generating and measuring techniques, both automated and manual, in heavily forested areas (Büyüksalih & Jacobsen 2004). This fact had to be taken into consideration when selecting sampling sites for elevation accuracy assessments.

Terrain captured in the ASTER scene is gently rolling, sub-Appalachian piedmont. Relief variation is rarely locally significant or abrupt relative to ASTER's 15 m X 15 m pixels and across the entire scene does not exceed 300 meters, with only a gradual average elevation rise of nearly that much from the southeast to northwest image corners. This geographic

phenomenon reflects the ancient geologic uplift zone along the southern end of the Appalachian Mountains running generally perpendicular to the average elevation rise (i.e. northeast to southwest) in the scene. Rivers and streams are numerous in the scene but are rarely accompanied by large, steep, or abrupt drainage walls. Since such features produce terrain breaks too immediate for 15m pixels to accurately model, the image area was appropriate for evaluating ASTER's photogrammetric potential, in spite of the frequently high forest canopies.

The vast majority of the scene is rural with an approximate 2:1 agriculture-to-forest land cover ratio (fallow cropland being classified herein as agriculture, Figure 4.1). Urban and/or developed land occupies only about 10 percent of the scene. The city of Athens (population 101,000; Bureau of the Census, 2000), where this research was conducted at the University of Georgia, is nearly centered in the scene. Numerous other smaller communities with populations ranging from a few hundred to a few tens of thousands also appear throughout. Lakes and wide, unobstructed rivers are also visible in the image under magnification.

Data Preparation and Rectification

When assessing the cartographic accuracy of topographic maps, three primary criteria are essential to the assessment: content, are relevant features represented?, position, are features represented in their correct locations?, and elevation, are features represented at their correct terrain heights? (Doyle, 1984; Light, 1990). When assessing the cartographic potential of sensors used to capture imagery from which topographic maps are created, the same three criteria apply. Since ASTER's 15 m X 15 m IFOV is inherently incapable of accurately modeling planimetric features with edges, corners, or dimensions at or below the ground pixel size, most features are necessarily "misrepresented" by an ASTER raster image. In actuality,

features almost always must be significantly greater than the pixel size since virtually never are perfectly square features of exactly a pixel's dimensions captured precisely at image pixel boundaries. However, the same can be said of all cartographic representations with respect to a sufficiently large map scale. The goal of an assessment of the ASTER sensor, then, as it would be for any sensor, is to constrain the definition of "accuracy" vis-à-vis cartographic potential to map scales relevant to those which a 15m pixel can reasonably model.

If content, position, and elevation are the three essential topographic accuracy assessment criteria then they can be applied to the two categories of topographic features, planimetric and hypsographic, mentioned in Chapter 2. Doyle (1984) and Light (1990) also refer to them as types of information. Assessing planimetric and topographic accuracy (i.e. cartographic potential), therefore, is ideally accomplished by measuring the three types of cartographic information against the real world information being modeled. Since making such comparisons is, depending on the methods used, somewhere between very time consuming, and therefore expensive, and impossible due to inaccessibility, reference data such as imagery of a much higher spatial resolution, maps of a much larger scale, and control points of a much higher geodetic accuracy than the data generated by the sensor being evaluated can be substituted for real world feature verification.

For this research all of the aforementioned reference datasets were used, each for a different accuracy assessment at a different phase of the project. When land use/cover classification accuracy was assessed, USGS digital aerial quarter quadrangle orthophotographic imagery (DOQQ) was employed to compare randomly selected points in the classified ASTER image to the corresponding points in the photography. In conducting the land use/cover classification of the ASTER data, Level I of the Anderson scheme was used because it was

appropriate for ASTER's 15-meter spatial resolution. When hypsographic accuracy was assessed, field-captured GPS points were employed to measure spot elevation accuracies, two reference DEMS were employed, one from the USGS and one from the SRTM to compare with the ASTER DEM (Figure 4.2), and manually traced USGS aerial photogrammetric contours were employed to compare with manually-traced orbital photogrammetric contours from the ASTER data.

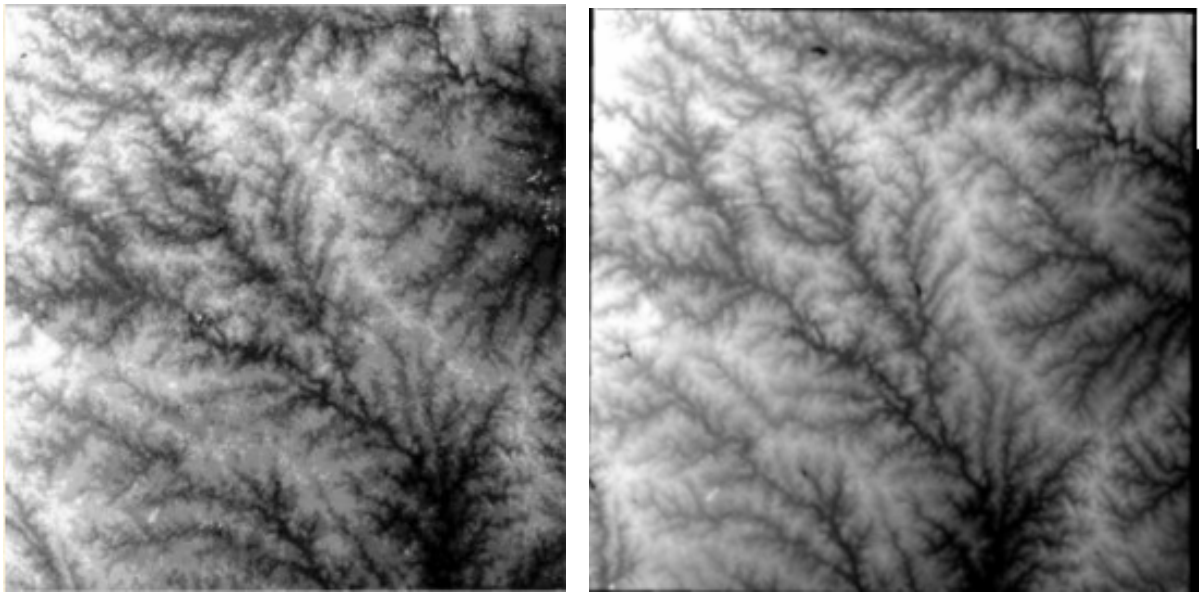

Figure 4.2: Reference DEMs. Left image: USGS; right image: SRTM.

The methods employed for the thematic and hypsographic accuracy assessment research conducted for this paper (thematic and topographic) were similar with respect to the preliminary work of image registration, i.e. image-to-ground orientation, but different with respect to the assessments themselves. The similarities consisted of a) rotating and reprojecting the imagery to match the reference data's coordinate systems and projections, and b) registering the imagery to measured ground control points. Rotating and reprojecting digital imagery has become a simple

process with modern digital image processing software but image-to-ground registration can be, depending on the imagery employed and the accuracies required, considerably more difficult and time consuming. Imagine software from ERDAS (v. 6.0) was employed for the thematic, or land use/cover classification, portion of this research while Desktop Mapping System (DMS) software was used for the photogrammetric portion.

Registration of the ASTER scene to ground, i.e. absolute orientation, or AO, for thematic classification involved the three VNIR bands (bands 1, 2 and 3N) of the image. Image-to-ground orientation for photogrammetric evaluation involved the stereomodel formed by bands 3N and 3B of the image. Each process required a well distributed network of reliable ground control points (GCPs) to be measured, i.e. interactively digitized, at image locations matching their conjugate ground locations.

For the thematic research, requiring less than VHR precision, image-to-ground registration first required rotating the original path-oriented image to match the reference dataset; a Digital Raster Graphic (DRG) mosaic of 20 1:24,000 scale USGS topographic quadrangles covering approximately 90 percent of the image area. The control points selected were fifteen clearly identifiable, well distributed benchmarks in the mosaicked DRGs matched to the conjugate locations in the ASTER image, a selection process more easily described than conducted since most USGS benchmarks are not clearly identifiable in 15m IFOV imagery.

Since the VNIR image was registered to the USGS topo benchmarks it required an initial projection during resampling which referenced the same horizontal datum used by USGS topo quads; the North American Datum of 1927 (NAD27). Since the thematic reference imagery, a mosaicked set of 1:6000 scale DOQQs, against which classified land cover features would be compared for classification accuracy, was projected into UTM coordinates (Zone 17N), using the

North American Datum of 1983 (NAD83), a re-projection of the registered VNIR image to the reference imagery projection and coordinate system was required.

This registration procedure, while somewhat tricky with respect to control point matching between the topo quad mosaic and the image scene, is limited to a two dimensional image-to-source data orientation. As such, a simple affine transformation of the image pixels from a self-referential orientation to a ground- , or source-referential orientation is all that is required to register the image, to be followed by resampling. Orienting and registering a pair of stereo images to ground is considerably more complicated, requiring first, a registration of the image to the sensor, i.e. internal orientation, second, a registration of the images to each other, i.e. relative orientation, and third, an orientation of the image pair to ground, i.e. absolute orientation.

One of the advantages of the DMS software is its simplification of these standard photogrammetric orientation steps. Relative orientation of ASTER stereopairs, however, requires a rotation of both images by 90° to create a stereomodel wherein pixel rows, rather than pixel columns, display parallactic separations, or X-parallax, due to terrain relief (Figure 4.3).

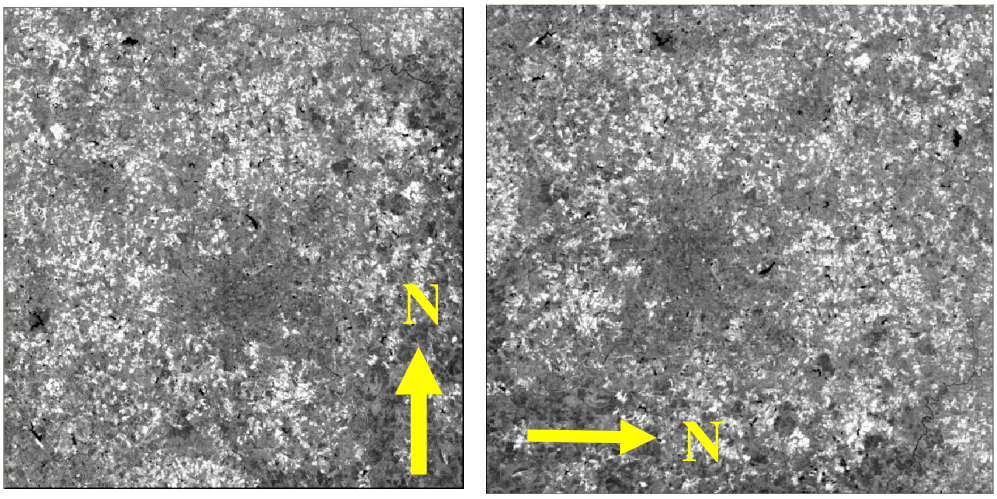

Figure 4.3: Rotation of ASTER Scene Required for Relative Orientation.

Once the images are rotated, relative orientation is accomplished by the measurement of identical points in each image. Figure 4.4 displays the ASTER scene overlain with hypothetical, well distributed image registration, i.e. control, points. The backward-looking sensor captures a longer image dimension due to its tilted look angle, illustrated with the dashed rectangle outlining the nadir image extents over the paired image.

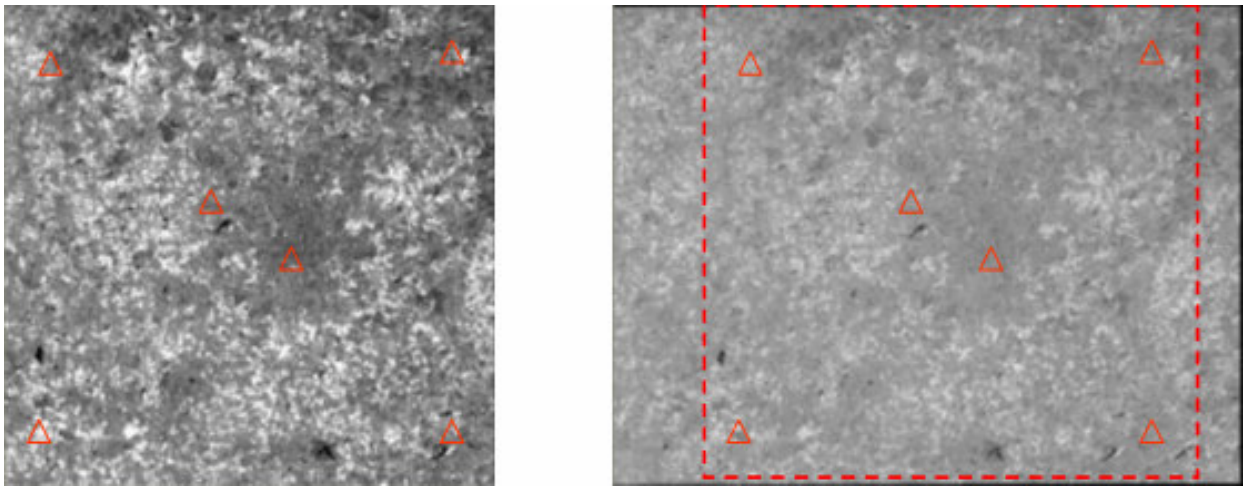

Figure 4.4: Hypothetical Image-to-Image Registration for Relative Orientation.

Since VHR precision was a prerequisite for the stereoscopic research, a hand-held Garmin GPS receiver was employed in the field to collect a network of 65 well-distributed GCPs throughout the image area. (Figure 4.5). The receiver was tested prior to field use to horizontal and vertical accuracies of ±4 m and ±5 m respectively, approximately three times the reported accuracy of ASTER VNIR datasets, against a network of eight First Order geodetic control points distributed around the UGA-Athens campus.

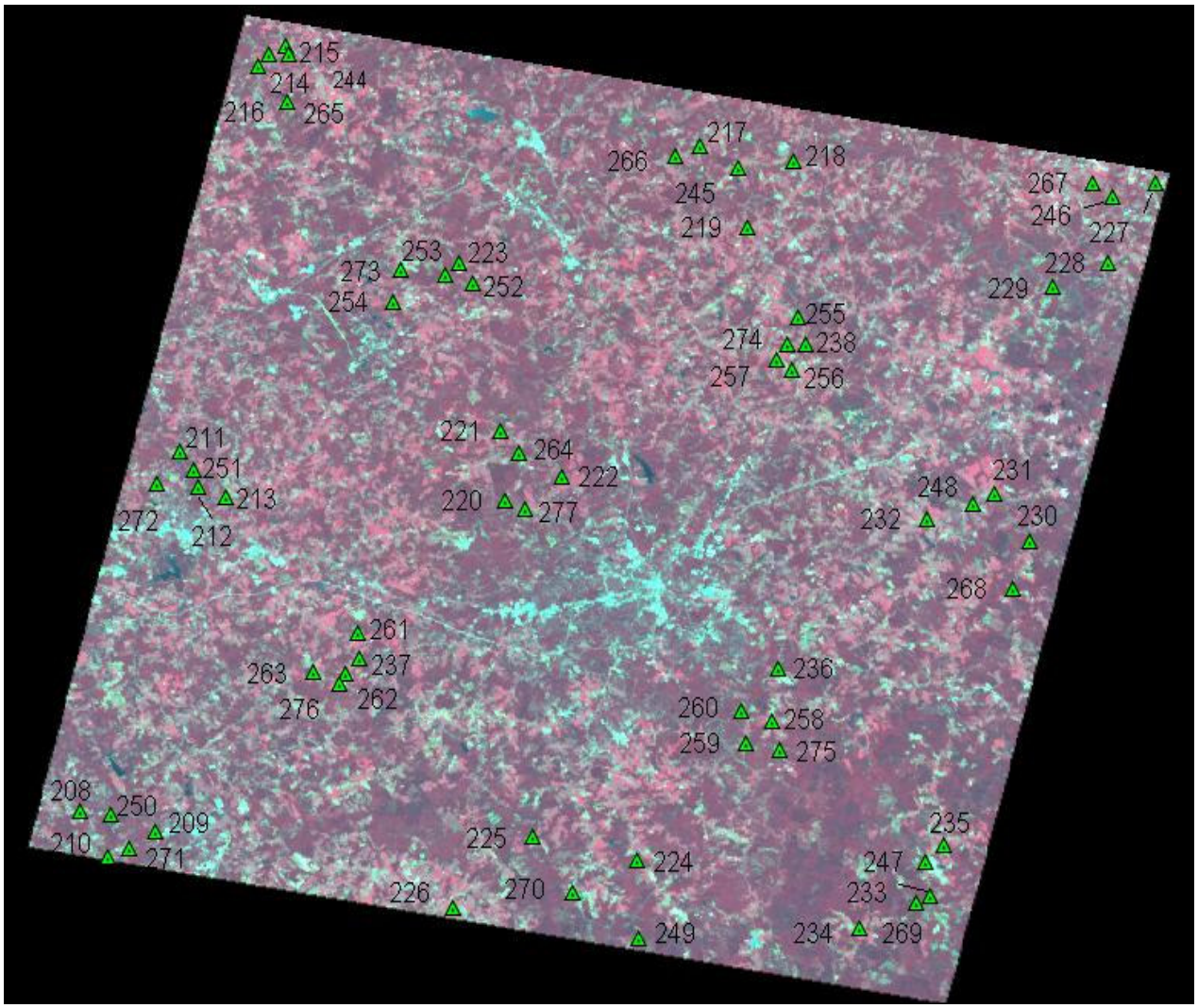

Figure 4.5: Stratified, Semi-Clustered GPS Ground Control and Check Point Network Distributed Throughout the ASTER Scene Area. Note the necessary absence of GCPs from urban areas.

Like the benchmarks selected from the topo maps described above, 3-D GPS points required digitally interactive selection prior to field measurement from easily identifiable, precise locations in the magnified imagery so they could be matched to detailed map locations and found in the field. The difficulty of ground feature recognition from 15m pixels described above is amplified when only the grey scale images of bands 3N and 3B are viewed in forming the stereomodel (Figure 4.6). Fifteen-meter pixels, even in multi-band imagery, cannot easily

differentiate between many urban features where near-ubiquitous asphalt and concrete reflectance signatures from pavements and rooftops appear in a scene (Lo & Choi, 2004).

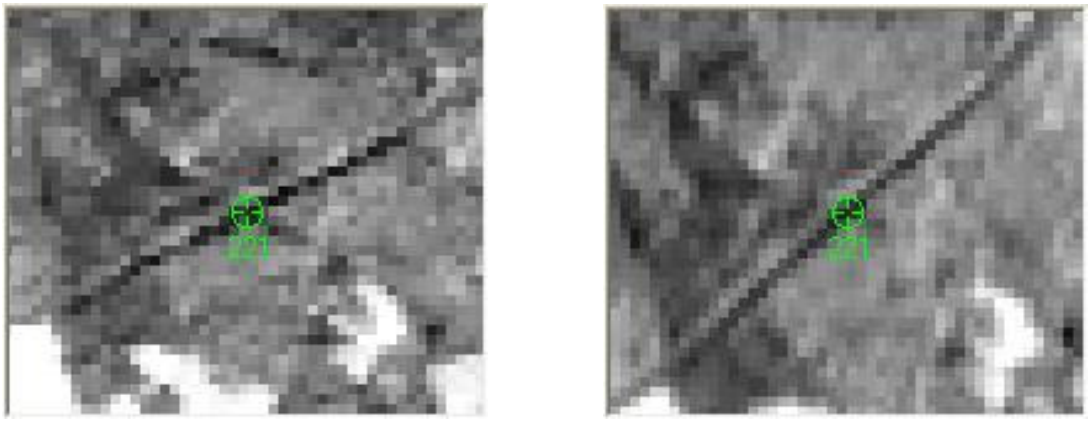

Figure 4.6: GPS Point 221 From Fig. 3 As Displayed Under Magnification in the Single-Band NIR Grey Scale Stereoscopic Image Pair. Note how the intersecting road is considerably less identifiable in the backward-looking image (right).

Limiting stereo capture bands to one effectively homogenizes pavement signatures in ASTER stereo imagery such that all urban features appear essentially identical. Rural road intersections, therefore, provided the most reliable, easily identifiable, and easily accessible locations for GPS point selection.

While a theoretical minimum of three XYZ GCPs is required to ground-orient a stereo image pair (Wolf & Dewitt, 2000, p. 286), at least twice that many are required for a reliable least-squares solution, which the DMS software provides. Additionally, a greater GCP density/redundancy enhances both overall, or pan-scenic, and restricted terrain modeling accuracies proximal to localized terrain perturbations. It also reduces the propagation and/or influence of input errors associated with the inevitable mis-measurements of control points (Toutin, 2004b).

After control point collection, a variety of GCP selection sets were tested during the stereoscopic AO, with diminishing returns, i.e. no-longer-decreasing orientation residuals, encountered at 14 specific, well distributed points used for the orientation solution. Ironically, certain points used in test ROs, when included in test AOs, increased orientation residuals despite being among the most accurate when withheld as check points. Since the goal of a stereoscopic orientation is to obtain the best orientation possible, the control points selected for the final AO were not identical to control points selected for the final RO (Figure 4.7). It should be noted that the two images were captured during test orientations using more than the final selection set of 14 GCPs.

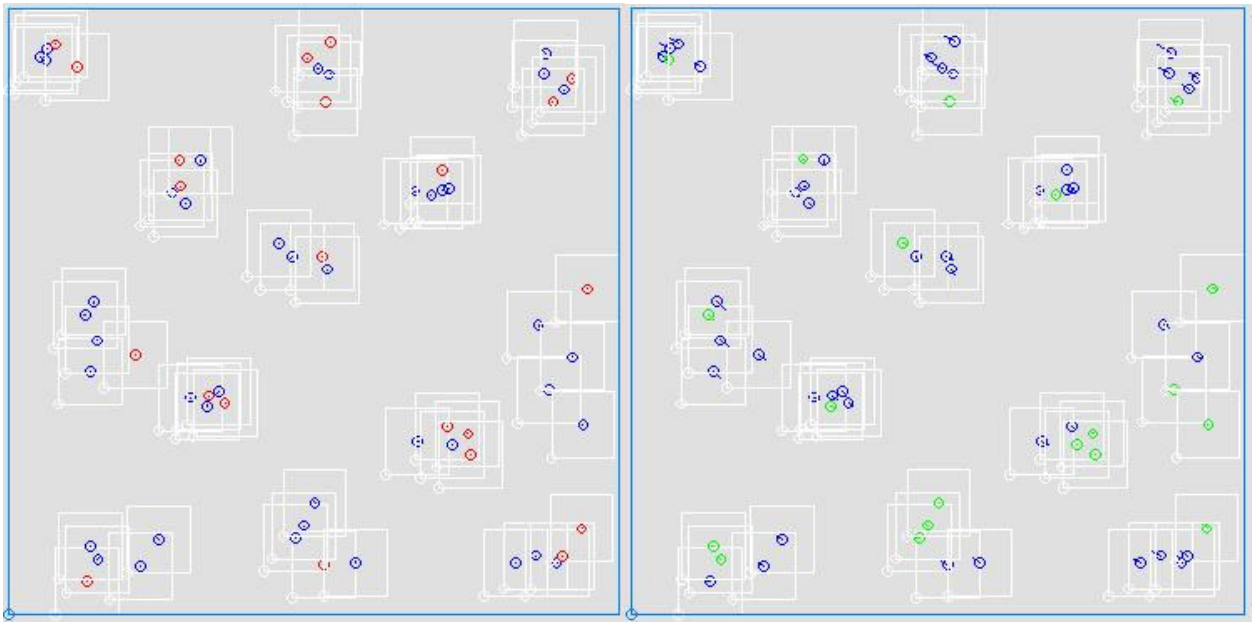

Figure 4.7: Relative (Epipolar) and Absolute (Ground) Orientation Residuals, Left and Right Respectively, Displayed Graphically by DMS as Vectors Pointing From Symbol Centers. Note the asymmetry between selected RO points (red) and selected AO points (green) reflecting the different point sets used in each orientation.

The 14 GCPs used for the final AO (14) were in general agreement with published photogrammetric assessments of ASTER and other satellite imagery (Hirano, *et al,* 2003; Cheng,

et al, 2003; Dowman & Michalis, 2003; Subramanian, *et al*, 2003;). The remaining 51 GCPs were withheld from the AO for use as accuracy assessment check points of the automatically generated DEM.

For the thematic (single image) orientation, once the map benchmarks were measured in the image, an automated first order affine polynomial transformation was performed on the image pixels to fit the map benchmark geometry, followed by resampling the image raster using the nearest neighbor method for spatial interpolation of pixel values. For the stereo orientation, once the GPS points were measured in the respective stereo images (monoscopically and individually in DMS), a second order transformation was required to relocate the image pixels to fit the GPS network geometry, followed by resampling the image raster using a nearest neighbor method for spatial interpolation of pixel values.

While many COTS digital photogrammetric orientation routines employ more complicated mathematical algorithms in the AO regimen, that process, greatly simplified, either solves for the six image orientation parameters ω (roll) φ (pitch), κ (yaw), x, y, and z by satisfying, through matrix algebra, the photogrammetric collinearity condition equations or it employs the first three of those six parameters from supplied sensor ephemeris data. One of the benefits of DMS software is its lower cost, employing a simpler absolute orientation algorithm with an integrated RO-AO approach. A virtual average-Z horizontal datum is calculated from input GCP_z values (or supplied from other source data) and used as a floating Pythagorean hypotenuse to compute each pixel's oriented x-y location based on the horizontal offset, or epipolarized X-parallax (dX), at that new location (Figure 4.8).

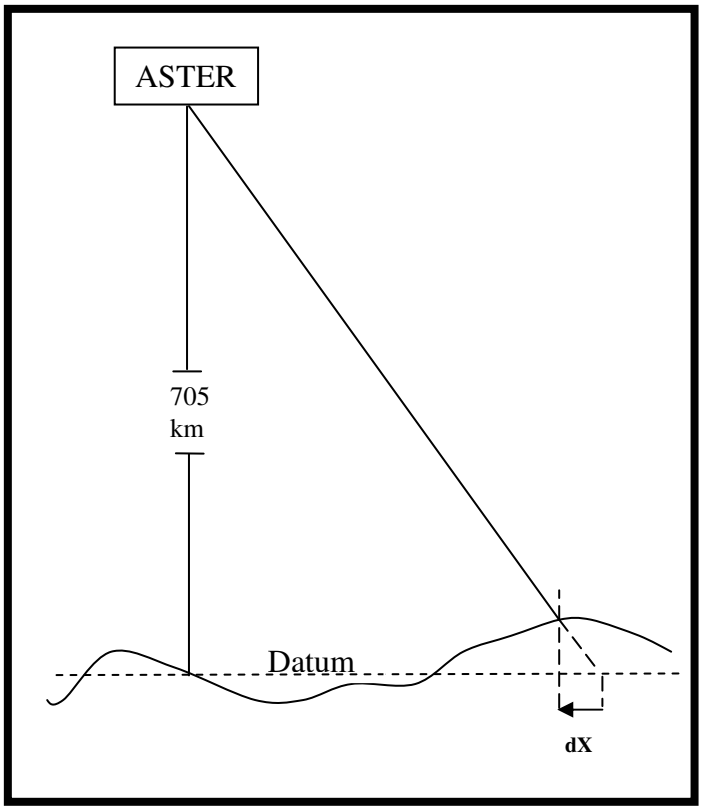

Figure 4.8: Diagram Showing an Artificial Datum Formed at the Average Elevation of the GCPs. Pixel coordinates are offset (dX) to datum based on terrain height (Z), position in image, and look angle of the ASTER sensor.

Such a simplified mathematical approach to stereoscopic orientation has the advantage of not requiring complicated optical central perspective collinearity solutions or sensor ephemeris data, though a backward look angle, which is constant on ASTER, is required. The approach, however, trades some predictability with respect to orientation accuracy vis-à-vis Earth curvature and the selection of polynomials used for pixel transformations. Earth curvature correction, quite relevant in 3,600 km^2 imagery, is not explicitly corrected by the DMS orientation algorithms, but can usually be eliminated with an available second order polynomial transformation. In fact, the first several attempts at stereo-orienting the project imagery failed due to the selection of a first order affine polynomial transformation that could not correct for

Earth curvature. A continuous along-track elevation anomaly, or "hump", in the first order-transformed, parallax-resolved pixels nearest to sensor nadir reflected the spherical distortion that affine transformations cannot remove (Figure 4.9).

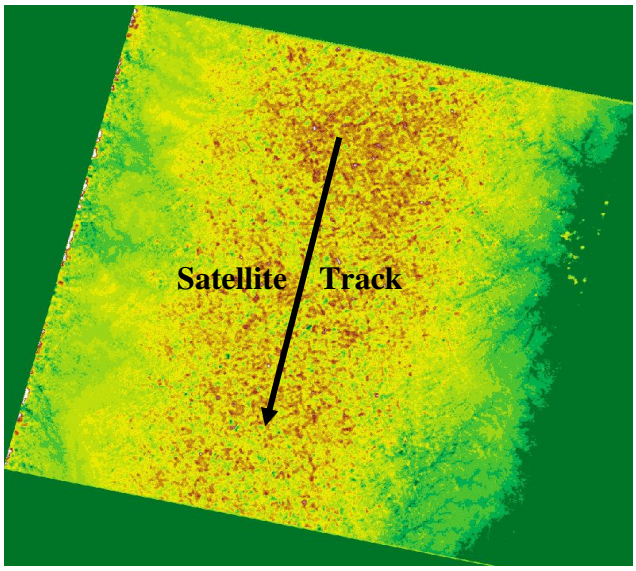

Figure 4.9: Colorized DEM Generated From a Test Orientation of the ASTER Scene Using a first Order Affine Polynomial Transformation. Note the "raised" elevations of pixels closest to nadir relative to those at lateral image edges.

Mathematically, the first order two-dimensional affine transformation employed by DMS to transform pixel coordinates for stereo orientation has the general form:

$$X_t = a + b(x_m) + c(y_m)$$

$$Y_t = d + e(x_m) + f(y_m)$$

where the variables x_m and y_m are the measured coordinates, the variables X_t and Y_t are the transformed coordinates, and a through f are coefficients. The eventual selection of a second order (quadratic) transformation proved to be mathematically robust enough to approximate

Earth's curvature, yielding an stereo orientation. The general mathematical form of the second order polynomial employed by DMS is:

$$X_t = a + b(x_m) + c(y_m) + d(x_m^2) + e(y_m^2) + f(x_m y_m)$$

$$Y_t = g + h(x_m) + i(y_m) + j(x_m^2) + k(y_m^2) + l(x_m y_m)$$

where, likewise, the variables x_m and y_m are the measured coordinates, the variables X_t and Y_t are the transformed coordinates, and *a* through *l* are coefficients.

When properly oriented, generation of a DEM is accomplished in DMS with the application of a stereocorrelation routine employing a mean normalized cross-correlation algorithm that compares reflectance values within a floating pixel matrix, or correlation window, between images (Figure 4.10).

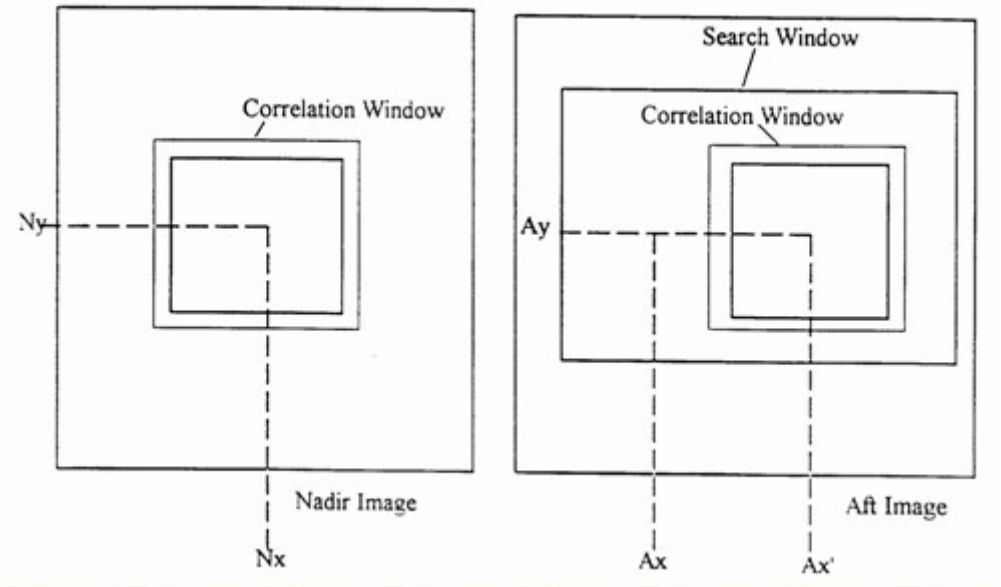

Figure 4.10: DMS Cross-Correlation Geometry for DEM Stereocorrelation.

A search window containing the correlation window searches one image until it finds a general match of reflectance values with a search window in the other image, then the correlation

window floats around the search window until a precise match is found. The correlation produces a pixel coordinate offset (dX; Figure 4.8) based on terrain height and an elevation is then computed for each correlated pixel. The new image is then resampled to the resolution, or posting dimensions, pre-defined by the user for the application at hand. In this case 30 m to compare post-by-post with reference DEMs of the same resolution.

Land Cover Classification

With registered/oriented imagery, the tasks associated with accuracy assessment were undertaken. The first such task with respect to thematic accuracy in land cover mapping was to apply ERDAS Imagine software to classify the reflectance signatures in the VNIR scene using Level I classes from the Anderson land cover classification. Imagine software offers several image classification routines to generate classified datasets and tools within those routines to enhance classification accuracies. Anderson Level 1 consists of the following land cover classes applicable to the Athens ASTER scene: urban, agriculture, range, forest, water, wetland, and barren. This process, known as supervised classification, required selecting training sites of known Level I land cover, and entering those signatures into Imagine's comparator database for a supervised classification. A maximum likelihood classifier, the most popular classifier, was selected.

Once the supervised classification was completed, 1000 randomly generated check points were examined in each of the three different, cursor-tracked views of the scene (Figure 4.11). One view displayed the reference DOQQ, another view the unclassified image, and a third view the classified image, all of which could be set and re-set to user-specified spatial extents, or

zooms. Any cursor placement in one view was real-time matched in the other views irrespective of spatial extents displayed in those views.

The process of accuracy assessment involved tabulating the classified vs. actual, or reference, land cover types at each of the check points. Check points that were uncertain or unidentifiable in the reference imagery were ignored. A variety of reasons for ignoring check points was encountered, such as point locations in the shade, on developing or otherwise changing land, at or near feature boundaries, or points that represented land cover types not listed

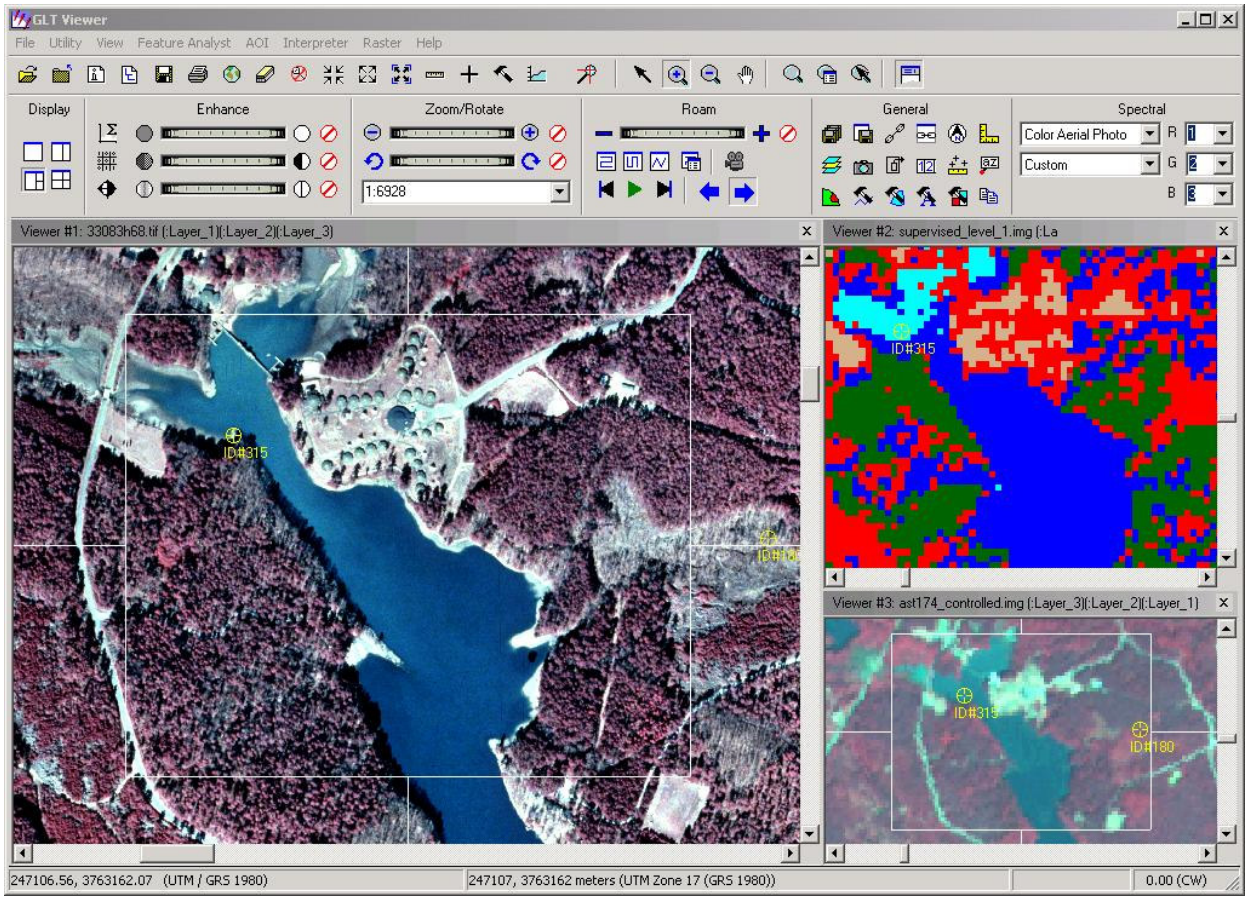

Figure 4.11: ERDAS Imagine Version 8.6 Geospatial Light Table GUI Allowing Multiple, Cursor-Linked Views of Identically Projected Raster Data. The views shown are an aerial DOQQ (left), a Level 1 classified image (top right), and the original ASTER VNIR scene (lower right). Note the two randomly generated accuracy assessment check points visible in the view area

in Anderson's Level 1 scheme. A total of 550 points were ignored in this assessment. An error, or confusion, matrix and a statistical report are generated by the software when all the check points have been examined.

A second classification technique, known as unsupervised classification, was also executed on the image to test whether it would be more or less accurate than the supervised technique. An unsupervised classification begins with the user pre-selecting a certain number of classes, usually several times more than the number of classes expected to be used in the results, into which the software places pixels by reflectance values. In ERDAS Imagine, unsupervised classification invokes an algorithm called Iterative Self-Organizing Data Analysis Technique (ISODATA) which delineates clusters of pixels with homogeneous reflectance values into the pre-defined classes. A manual aggregation of the ISODATA clusters into new classes by relating them to the land cover types identifiable in the reference imagery, highlighted graphically when selected from the table, completes the classification. Land cover types at usable check points are tabulated and a statistical report and error matrix are generated, just as with a supervised classification (402 of 1000 check points were ignored in this assessment).

Topographic Mapping

The research tasks associated with assessing the accuracy of ground elevations derived from ASTER stereopairs involved both manual and automated processes. The first of these tasks was to manually read and measure in stereo each of the 50 GPS points witheld from the orientation solution. Digital Mapping System employs the anaglyphic approach to stereo display and viewing. While both of the oriented images are projected on the same screen, one image is

projected through a digital red filter and the other through a digital blue filter. The user wears eye glasses with a red lens over one eye to view the red image and a cyan lens over the other eye to view the blue image to obtain the stereoscopic (3D) view. When all 51 points were measured, an $RMSE_z$ for the check point dataset vs. the GPS coordinates was calculated.

The second topographic assessment task required the automated generation of a DEM to compare with USGS and SRTM DEMs of the scene area. A DEM of the entire scene area was first generated with a 30 m post spacing, half the original ASTER image resolution (Figure 4.12, left image).

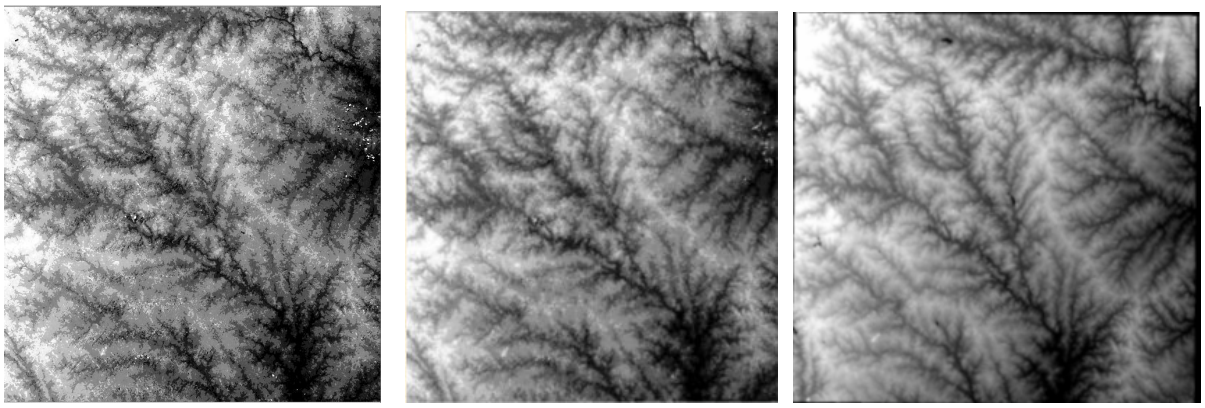

Figure 4.12: Full Scene DEMs. Left image: ASTER, center image: USGS, right image: SRTM.

Three DEM AOIs were selected from the scene representing the most prevalent Level 1 land cover classes defined in the supervised classification to examine whether significant differences in DEM accuracies would be discovered between them. The AOIs were relatively large in areal extent and were primarily characterized by the land cover classes by which they were named. The thee primary land cover classes selected for DEM AOIs were Urban/Residential, influenced by tree canopies and multi-storied buildings, Agricultural,

occasionally influenced by tree canopies, and Forest, occasionally interrupted by open space ground.

If the DEM post spacing exceeds the image pixel size (as it did in this project), multiple pixel elevation values for each DEM posting are averaged for the final post elevation. Since the reference USGS and SRTM DEMs were both delivered with 30 m post spacings, the ASTER DEMs, one from each AOI, were programmed to generate with the same posting dimensions, resulting in a numerical average of four 15 m pixel elevations for every DEM post. Precise corner coordinates from each DEM AOI were located on the USGS and SRTM DEMs to match spatial extents of the AOIs and all nine DEMs, three from each of the three AOIs, were spatially normalized by resampling to match each other post for post. A comparison routine resident in DMS was then run on the entire extents of the spatially identical DEMs rather than comparing only sampled postings along transects.

The third topographic accuracy assessment task was the least reliable, involving the manual digitizing of contours, but was executed to test whether the 40 m-50 m contour interval thresholds prescribed for ASTER imagery by Hirano, *et al*, (2003, p. 369) and Wolf & Dewitt (2000, p. 413) could be reduced. Digitized contours were collected at half that threshold (20m intervals) to compare with USGS contours of the same interval; 40m-50m contours, more typical of high relief terrain maps, were unavailable for the scene area. Comparisons of the digitized contours with the reference contours were made by measuring nearest perpendicular, horizontal distances from each contour encountered along a cross section line to its referent and plotting those distances on a scattergram vs. the number of contours encountered. The cross section lines were oriented to cross as many contours as possible. The median and standard deviation of distances between digitized contours and their referents, as well as the number of countours

existing on the reference map but not digitized and the number of contours digitized but nonexistent on the reference map, all of which were closed contours representing terrain crests or depressions, were also recorded on the plot.

Chapter 5

Results of Accuracy Assessment

Thematic Accuracy of Land Cover Image Map

Land cover classification, especially of the supervised approach using the maximum likelihood classifier, with 15 m IFOV data is characterized by several common problems. First, pixels often contain multiple, or mixed, signatures reflecting off of different surface types resident in the pixel footprint (Jensen, 2000). Second, sensors do not often possess adequate spectral and/or radiometric resolution to separate signatures (Jenson, 2000). Third, features themselves, i.e. land cover types, do not reflect consistent, identical signatures. All of these problems existed in the scene classified and analyzed for this thesis (Figures 5.1 – 5.3).

One of the classification problems described above can be dramatically demonstrated graphically. While water was not a significant percentage of the total scene area (reservoirs, rivers, and wetlands were all present but comprised less than 5 percent of the scene), the spectral confusion between water body signatures and between water and other land cover signatures, primarily pavement and barren land, was quite high. Several attempts at re-training the comparator made little improvement. Examination of several water features revealed the nature of the problem (Figure 5.3).

Since the Anderson scheme does not differentiate between hydrologic land cover categories of greater and lesser turbidity, bathymetry, sensor and/or solar angle, or surface wind

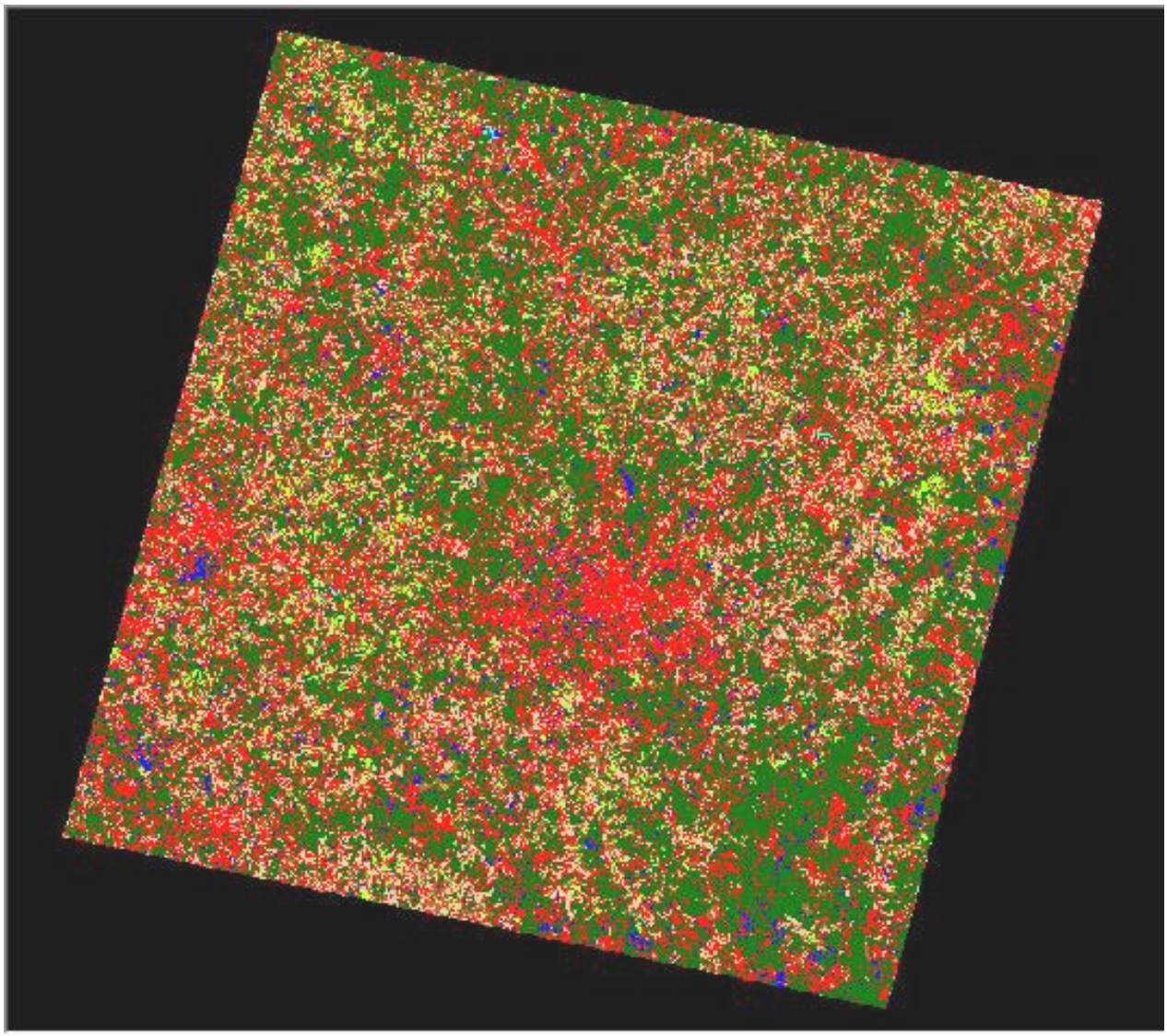

>	Signature Name	Color	Value
>	Urban		2
	Crops		3
	Range		4
	Forest		5
	Deep/Clear Water		6
	Barren		7
	Shallow/Silty Water		1

Figure 5.1: Full Scene Image Map of Unsupervised ISODATA Classification. Color legend appears at right. Note the city of Athens slightly right and below center and the significant number of misclassified Urban pixels throughout the rest of the primarily rural scene area, reflected in the low Users Accuracy, Table 5.2.

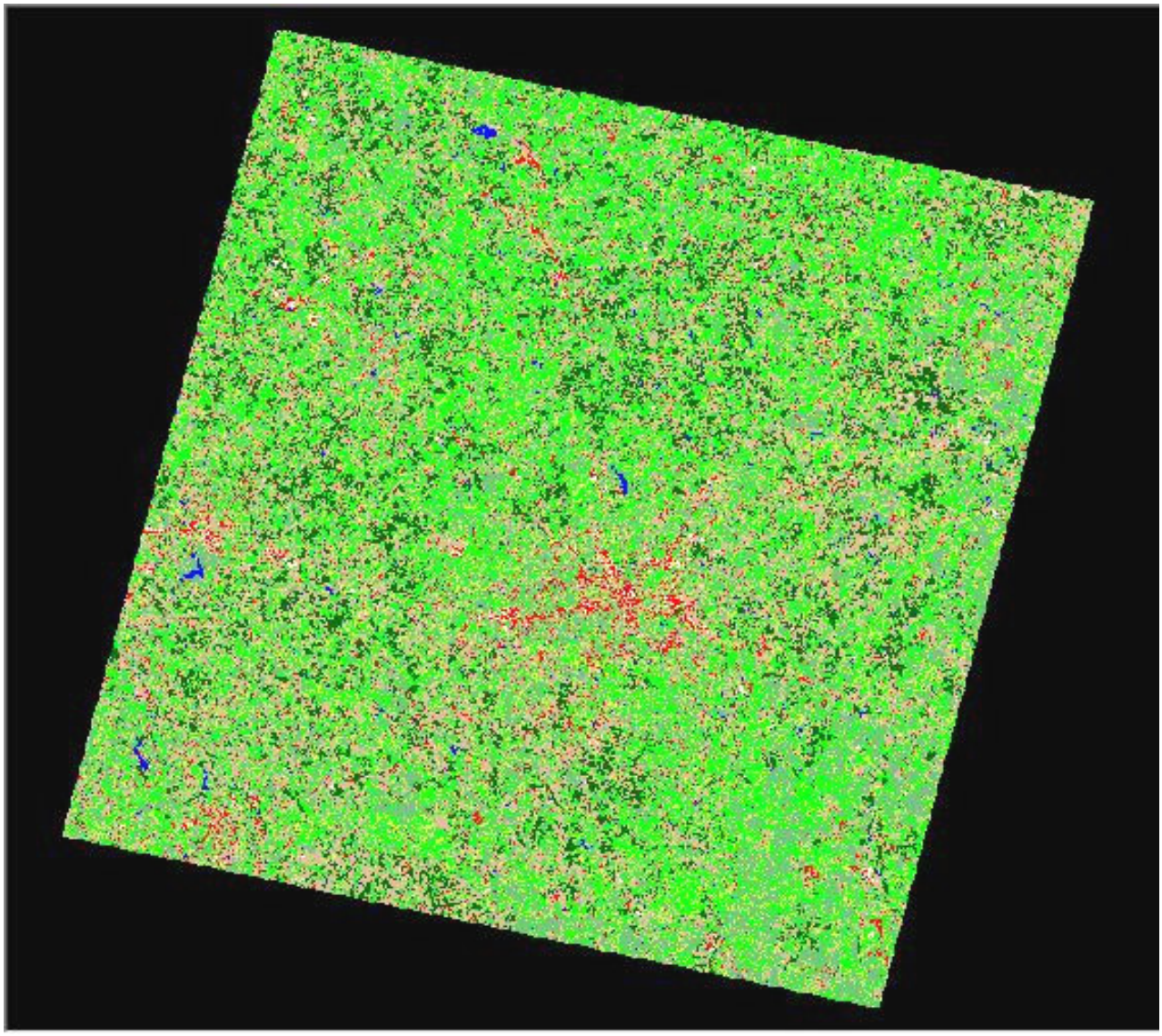

>	Signature Name	Color	Value
>	Water		8
	Deciduous Forest		1
	Coniferous Forest		2
	Mixed Forest		3
	Asphalt/Gravel/Clay		4
	Concrete/Metal/Non-Clay Soil		5
	Crops		6
	Range/Pasture/Grassland		7

Figure 5.2: Full Scene Image Map of Supervised Anderson-based Level 1 Classification. Color legend appears at right. Note the preponderance of forest land covers in the scene area suggesting a much improved overall classification would have resulted if a single forest class had been defined.

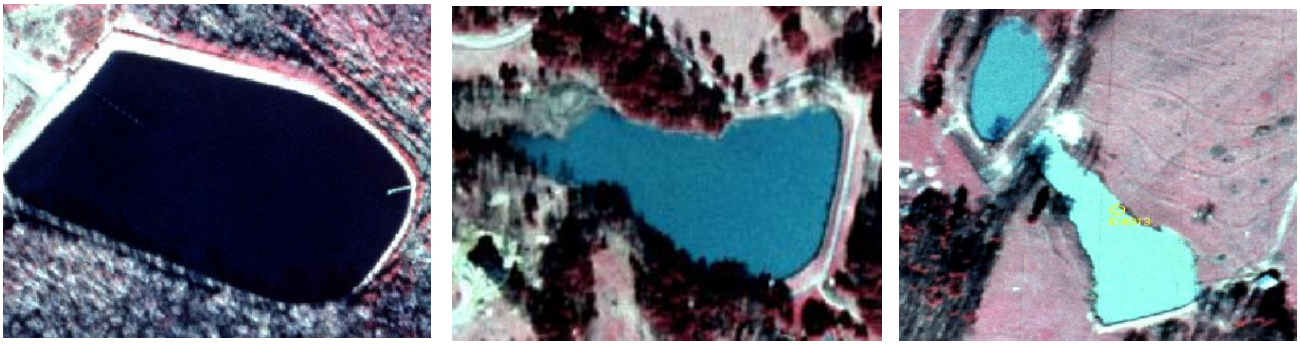

Figure 5.3: Four Different Reservoirs From the Research Scene. Viewed in DOQQs, the images display the wide range of spectral signatures captured from water features.

disturbance, each of which dramatically alters the wavelengths of reflected light from the surface of such features, attempts at training Imagine's histogram comparator to recognize such a wide variety of signatures as those displayed in Figure 5.3 as a single land cover class proved futile. This problem with ASTER has been described by Zhu and Blumberg (2002) as well, citing spectral confusion in that study with various pavement features. Modifying the Anderson scheme to allow for differentiated water features, in this case shallow and/or silty water as one class and deep and/or clear water as another class, solved the problem completely. When a single water class was defined by the supervised classification, the percent of water pixels correctly classified was below 50 percent. When separate water classes were defined, effectively modifying the Anderson scheme to accommodate the capabilities of ASTER, a combined percent correctly classified over 90 percent for water pixels was realized (Table 5.2).

Note from Table 5.2 that, while the producers accuracies of shallow/silty water and deep/clear water were very high, the users accuracy of deep/clear water was only marginally improved over the original Anderson's scheme. Producers accuracy measures errors of omission and users accuracy measures errors of commission (Lo & Yeung, 2002). Virtually all of the errors of commission in that class were traceable to confusion with forest signatures. The overall

Table 5.1: Accuracy Assessment Confusion Matrix for Modified Anderson *et al* Level 1 Supervised Classification

	Reference Data						
Classified Data	Shallow/Silty W	Urban	Crops	Range	Forest	Deep/Clear W	Barren
Shallow/Silty W	49	0	0	0	0	2	0
Urban	0	23	1	2	22	0	23
Crops	0	0	45	10	1	0	0
Range	0	2	7	42	0	0	1
Forest	0	0	0	0	116	0	0
Deep/Clear Water	1	0	0	0	21	29	0
Barren	0	4	0	7	2	0	4
Column Totals	50	29	53	61	162	31	28

Table 5.2: Accuracy Totals

Class Name	**Reference Totals**	**Classified Totals**	**Number Correct**	**Producers Accuracy**	**Users Accuracy**
Shallow/Silty Water	50	51	49	98.00%	96.08%
Urban	29	71	23	79.31%	32.39%
Crops	53	56	45	84.91%	80.36%
Range	61	52	42	68.85%	80.77%
Forest	162	116	116	71.60%	100.00%
Deep/Clear Water	31	51	29	93.55%	56.86%
Barren	64	53	40	62.50%	75.47%
Totals	450	450	344		

Overall Classification Accuracy = 76.44%

Overall Kappa Statistics = 0.7160

Table 5.3: Conditional Kappa for Each Class

Class Name	**Kappa**
Shallow/Silty Water	0.9559
Urban	0.2774
Crops	0.7773
Range	0.7775
Forest	1.0000
Deep/Clear Water	0.5367
Barren	0.7140

accuracy of the supervised classification was about 76 percent with a Kappa statistic of 0.716.

The next task was to use ERDAS Imagine software to perform an unsupervised image classification. As has been explained in Chapter 4 above, the unsupervised image classification based on the ISODATA method delineates clusters of homogeneous pixel values, i.e. spectral reflectance values, which are then manually interpreted with reference to the ground truths extracted from the DOQQs into meaningful land cover classes. Figure 5.4 displays spatially similar sections of the ASTER scene for comparison. The display colors chosen for the two

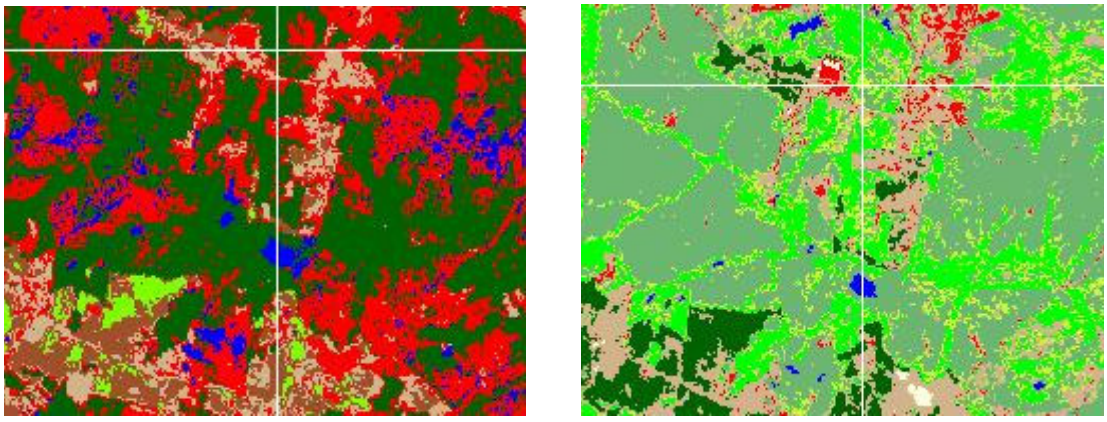

A) Supervised Level 1 sub-scene.

B) Unsupervised Level 1 sub-scene.

>	Signature Name	Color	Value
>	Urban		2
	Crops		3
	Range		4
	Forest		5
	Deep/Clear Water		6
	Barren		7
	Shallow/Silty Water		1

>	Signature Name	Color	Value
>	Water		8
	Deciduous Forest		1
	Coniferous Forest		2
	Mixed Forest		3
	Asphalt/Gravel/Clay		4
	Concrete/Metal/Non-Clay Soil		5
	Crops		6
	Range/Pasture/Grassland		7

Figure 5.4: A Typical Multi-Class Area From Each of the Classifications. Note the spatially identical (syncrhonized) cursor locations, a useful tool for many of the tasks performed with Imagine software.

classifications were purposely dissimilar in vegetation classes to avoid confusion over which classification was being viewed when multiple classifications were being simultaneously displayed.

Figure 5.4B displays many of the obvious improvements obtained with the unsupervised classification displayed in Figure 5.4A. Those improvements were more than merely graphical, as Tables 5.4 - 5.6 indicate. Several items are worth noting. First, what required separating into two classes for the supervised classification of water to be of any use was accomplished to an even higher degree of accuracy with a single class in the unsupervised classification. Note, specifically, the users accuracy of 100 percent. Second, what was intentionally separated into three classes in the unsupervised classification (deciduous, coniferous, and mixed forests) was classified to a significantly higher accuracy, albeit less explicit class, with a single class in the supervised classification. Third, aggregating certain urban, non-vegetative, non-water signatures in the unsupervised classification led to some rather confused titles for classes, for example Asphalt/Gravel/Clay Soil and Concrete/Metal/Non-Clay Soil, field verified in several locations in and around Athens, where those same signatures in the supervised classification led to some rather confused pixels (i.e. lower classification accuracies) instead. Which leads to the fifth point: the overall accuracy, or percent correctly classifiec (PCC), of the unsupervised classification was about 83 percent, or about 7 percent higher than the supervised classification. However, a second look at the three forest classes in the unsupervised error matrix reveals that virtually all of the signature confusions in those categories were from other forest classes. Since forests in the scene area were rarely completely monolithic by class, containing at least occasional representatives from species of both types of trees in a large percentage of forested areas, clearly visible in the leaf-off NIR DOQQs, the mixed pixel problem apears to have had

Table 5.4: Accuracy Assessment Confusion Matrix for the Supervised Classification

	Reference Data							
Classified Data	Deciduous Forest	Coniferous Forest	Mixed Forest	Asphalt/ Gravel/Clay	Concrete/ Metal/Non-Clay Soil	Crops	Range/ Pasture/ Grassland	Water
Deciduous Forest	87	0	16	0	0	1	3	0
Coniferous Forest	11	38	13	0	0	0	2	0
Mixed Forest	10	1	54	0	0	1	4	0
Asphalt/Gravel/Clay	0	0	1	60	4	0	10	4
Conc/Metal/NC-Soil	0	0	0	2	50	0	0	1
Crops	0	0	0	0	0	47	5	0
Range/Pasture/Grass	2	2	1	6	1	1	108	0
Water	0	0	0	0	0	0	0	52
Column Total	110	41	85	68	55	50	132	57

Table 5.5: Accuracy Totals.

Class Name	**Reference Totals**	**Classified Totals**	**Number Correct**	**Producers Accuracy**	**Users Accuracy**
Deciduous Forest	110	107	87	79.09%	81.31%
Coniferous Forest	41	64	38	92.68%	59.38%
Mixed Forest	85	70	54	63.53%	77.14%
Asphalt/Gravel/Clay	68	79	60	88.24%	75.95%
Conc/Metal/NC-Soil	55	53	50	90.91%	94.34%
Crops	50	52	47	94.00%	90.38%
Range/Pasture/Grass	132	121	108	81.82%	89.26%
Water	57	52	52	91.23%	100.00%
Column Total	598	598	496		

Overall Classification Accuracy = 82.94%

Overall Kappa Statistics = 0.8016

Table 5.6: Conditional Kappa for Each Class

Class Name	**Kappa**
Deciduous Forest	0.771
Coniferous Forest	0.5638
Mixed Forest	0.7336
Asphalt/Gravel/Clay	0.7286
Conc/Metal/NC-Soil	0.9377
Crops	0.8951
Range/Pasture/Grass	0.8621
Water	1.0000

an effect on these classes. Had the three forest classes been concatenated into one, the PCC for the unsupervised classification would have been over 90 percent.

An additional observation relating to classification methodology should be made regarding the aforementioned classification accuracies, and it is not explicitly visible from the accuracy reports themselves. The rudimentary supervised classification employed for this research was object-based in the sense that the classifying routine was trained to search for pixel signatures representing certain objects, or land cover, types, but it was more generally pixel-based in the sense that the routine then classified individual pixels based on radiance signatures alone. The unsupervised ISODATA clustering method is a rudimentary type of object-based classification which, in more robust forms, is capable of geometrically extracting feature forms and textures from pixel clusters. Since object-based classification methods have been shown to be generally superior to pixel-based methods of classification (Oruc, *et al*, 2004), it is not surprising that the ISODATA clustering method superceded the manually trained method used in this project.

Topographic Mapping Results

Orientation of the stereopair resulted in an average residual, actually an $RMSE_x$, of just under ±15 m. This figure was almost identical to the pixel dimensions of the dataset, but not as precise as others have achieved with the same software (Hirano, *et al*, 2003; Jordan, *et al*, 2005). Comparison of 50 check point coordinates measured in the oriented stereomodel against the reference GPS coordinates yielded an overall root mean square error for height ($RMSE_z$) of ±11m.

Results from the comparison of ASTER DEMs (Figure 4.12) generated from selected AOIs defined by the most prevalent Anderson land cover classes in the scene confirmed the expectation that first surface reflectance signatures from tree canopies would adversely affect the accuracy of ground measurements (Table 5.7). Review of 5.2 illuminates the prevalence of tree canopies encountered in the scene and how significant that prevalence would be expected to impact an overall, or pan-scenic, DEM accuracy. This prevalence of forest canopies led to the selection of land cover-based AOIs for DEM comparisons (Table 5.7).

Table 5.7: USGS and SRTM DEMs Compared to ASTER DEMS in Three Land Cover Classes, Post by Post.

ASTER DEM AOIs vs. USGS	RMSEz	ASTER DEM AOIs vs. SRTM	RMSEz
Urban/Residential	±10m	Urban/Residential	±11m
Agricultural	±12m	Agricultural	±9m
Forest	±35m	Forest	±11m

Unlike any of the studies cited above, this project compared entire DEMs to each other rather than selected postings along transect lines. Since each DEM AOI was geographically identical in extent to the others, the same number of postings (145,464) were compared in all nine DEMS. It is clear from the results (Table 5.7) that tree canopies affected the accuracies of both the ASTER and the SRTM DEMs since terrain modeling radar bands can penetrate cloud cover and some leaves but are reflected by more dense, woody tree trunks and heavy branches (Jensen, 2000). This probably explains the low Forest $RMSE_z$ (±11 m) comparing the ASTER

DEM to the SRTM DEM since radar is being reflected by woody masses below leaf canopies but above ground surface.

Surprising about these results was the lower $RMSE_z$ vs. the USGS DEM in primarily urban and residential areas (±10 m) than in primarily agricultural areas (±12 m). Since there was more expected bare earth or very low crop canopies in agricultural areas it was expected that lower comparative $RMSE_z$s would result, yet such was not the case with the USGS DEM comparison. Perhaps the influence on the ASTER DEM of high forest canopies surounding and between crop fields was greater than the influence of potentially younger, shorter tree canopies in built up areas. The ASTER/SRTM DEM comparison did produce a lower $RMSE_z$ (±9 m), in fact the lowest of all the comparisons made.

Selection of contouring sites within the scene was problematic due to two primary factors. First, there was a simultaneous need for a) terrain relief in excess of 40m in order to collect multiple contours for comparison since contours collected in flat areas are essentially incomparable due to their wandering variability and b) the need for bare earth terrain in those areas so that first-surface reflectances from high forest canopies would not be digitized as ground. This first surface reflectance effect was shown in the DEM results above to detract from accurately measuring ground surface elevations with ASTER imagery. Since terrain with the most relief also tended to be forested, the opportunities for ideal contouring sites were rare. Two contour collection areas were eventually selected, though neither was ideal. One area included the Athens central business district (CBD) and the UGA campus while the other, north of the city, was a more extensive area of mixed agricultural and forested land (Figure 5.5).

The cross section lines used to locate digitized contours from which perpendicular distance measurements to their referents are displayed in the figure as. A close-up of the

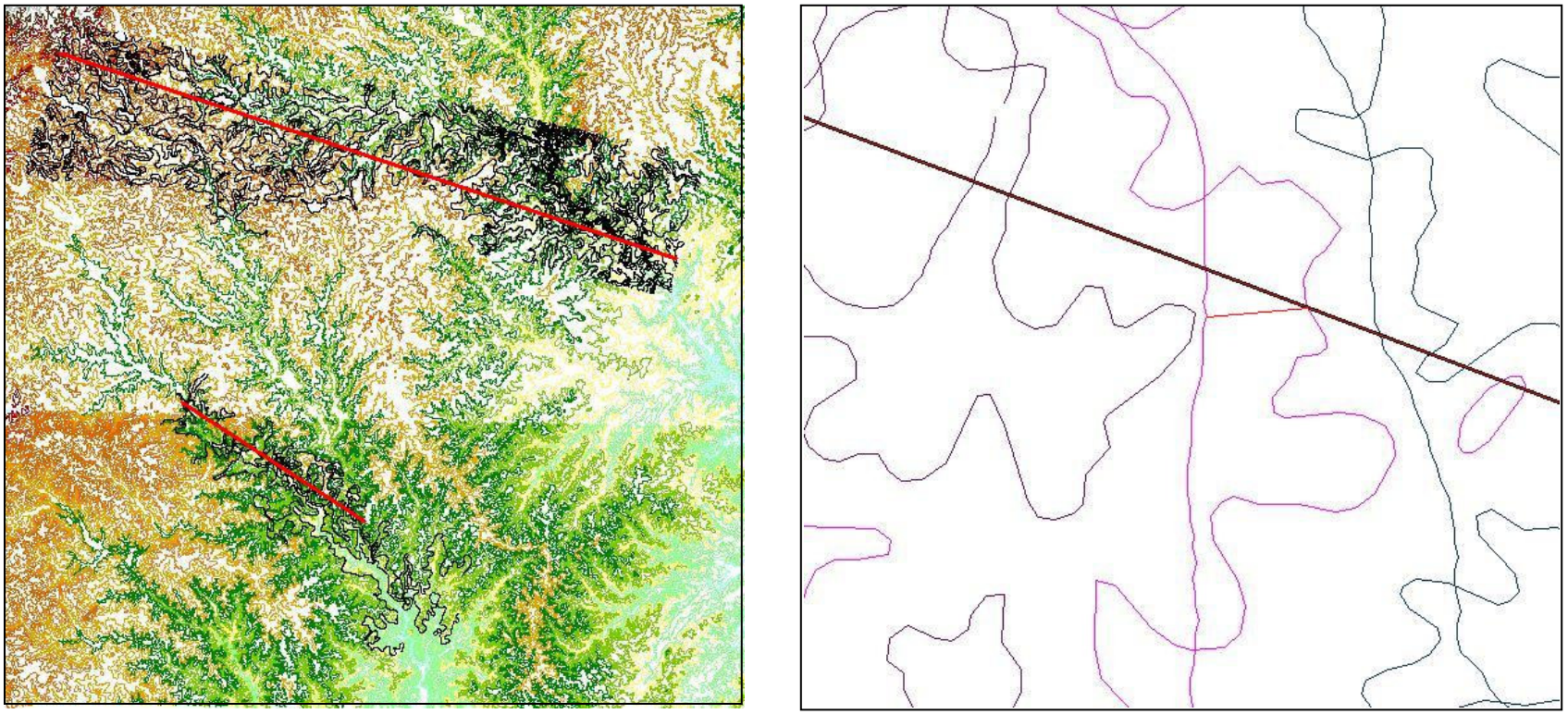

Figure 5.5: Cross Section Lines Through Contours Selected for Statistical Comparison with Stereo-Digitized ASTER Contours. Left image shows entire Scene area with reference USGS 20 m contours in color and ASTER contours in black. Right image shows a close-up of the cross section as it encounters a reference contour and the nearest perpendicular distance from that contour to the same-elevation ASTER contour. Contours of identical elevation, both reference and digitized, are colorized identically in the right image.

northeast portion of the scene area appears in Figure 5.6, providing a more detailed graphical comparison of the two contour sets. Contours were color matched in the display by elevation such that contours in the digitized set matched the colors of the same-elevation contours in the reference set. Not surprisingly, the more detailed contours in the figure were referents while the more generalized contours were digitized from the ASTER stereopair. It is clear from Figure 5.6 that, while general landform shape was accurately modeled with manual stereoscopic technique from the ASTER imagery, precise 20 m interval contour matching was not achieved. This interpretation of the figure is confirmed by the statistical plot of distances between digitized and referent contours in Figure 5.7.

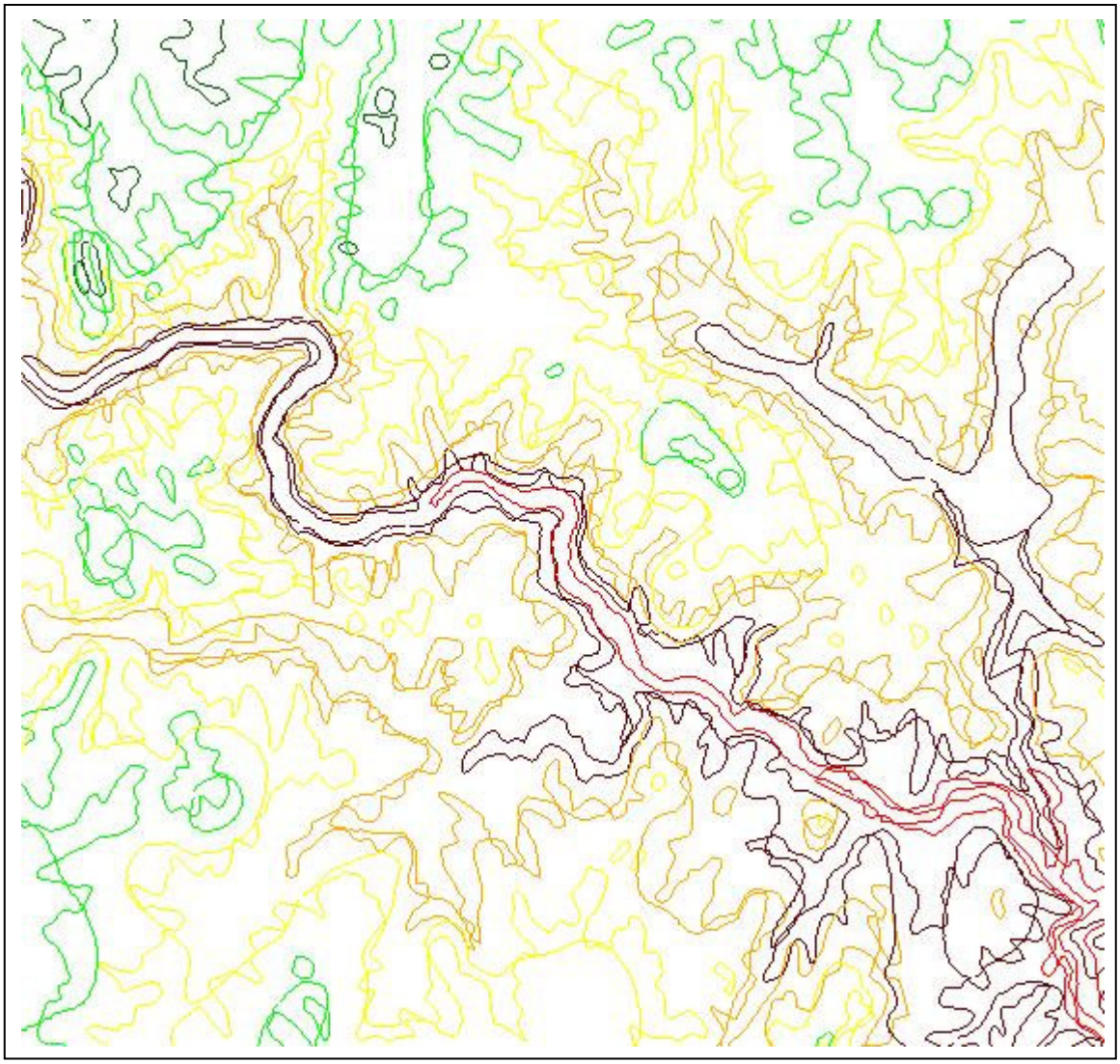

Figure 5.6: Graphical Comparison of Digitized and Reference Contours. Each elevation is represented by a different color with both contours at each elevation displayed in the same color.

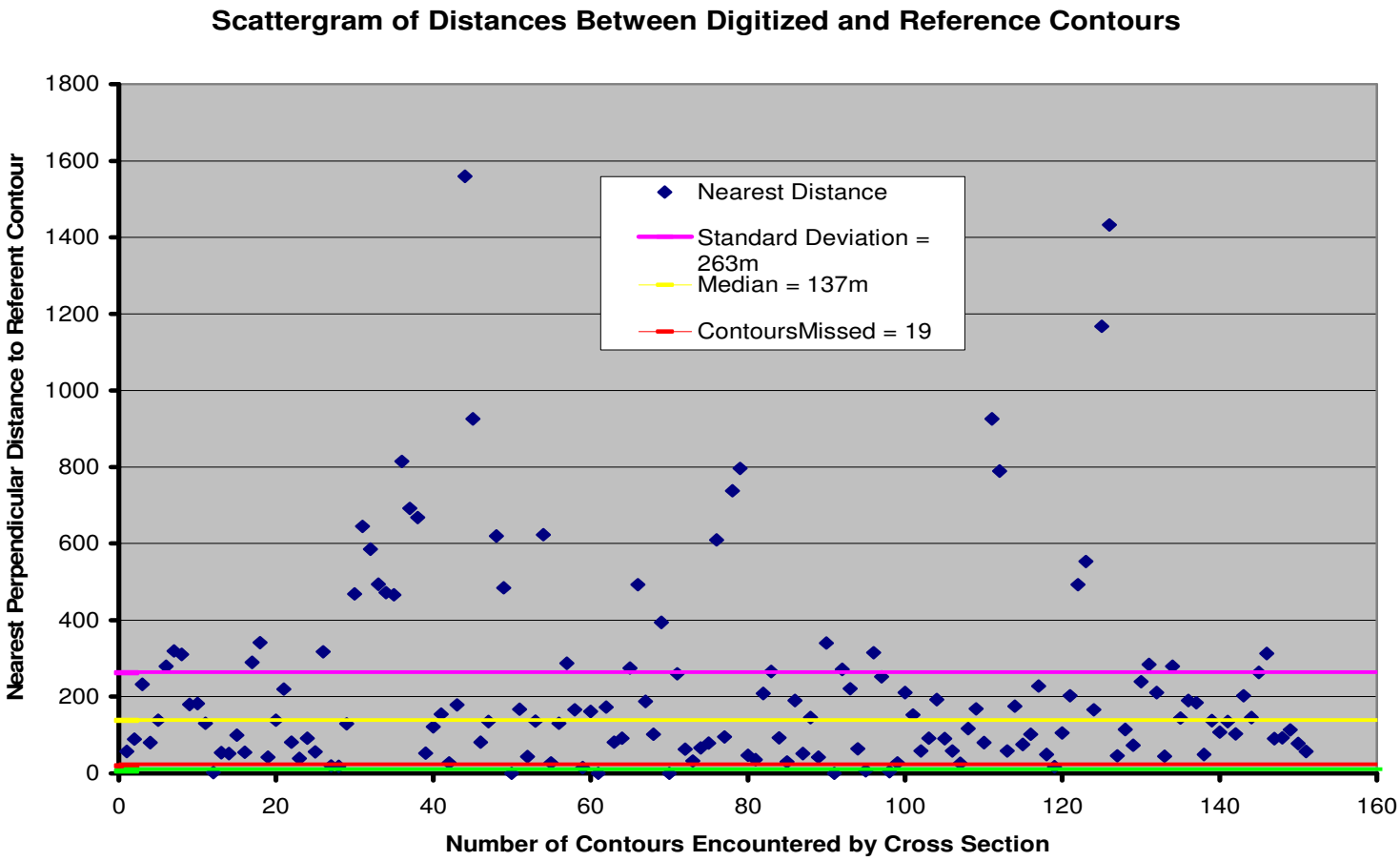

Figure 5.8: Scattergram of Distances Between Digitized and Reference Contours. Figure depicts nearest distances between digitized and feference contours, standard deviation of distances, median of distances, number of closed crest and/or depression contours missed, and number of closed crest and/or depression contours added.

Chapter 6

Conclusions

The stated goals of the research for this thesis were to assess the cartographic potential of ASTER VNIR data by determining their positional and height accuracies for topographic mapping and their thematic accuracy for the extraction of land cover information. After conducting the experiments described in previous chapters, the following conclusions can be drawn.

Thematic Accuracy

The supervised approach using the maximum likelihood classifier produced an overall accuracy of 76.44 percent and a Kappa of 0.716 for Anderson Level I land use/cover classes, which is below the 85 percent minimum accuracy requirement stipulated by Anderson *et a*l (1976). On the other hand, by using an unsupervised classification approach using ISODATA to delineate homogeneous clusters of spectral values, which can be manually labeled with reference to the "ground truth" image, it was possible to separate forest into three broad classes, deciduous, coniferous, and mixed, and urban into specific construction material classes, asphalt/gravel/clay, concrete/metal/non-clay soil, achieving an overall accuracy of 82.94 percent and a Kappa of 0.8016. These are similar to Level II land use/cover classes. These Level II classes of course can be re-combined into Level I classes, thus greatly improving its Level I accuracy.

Topographic Mapping

Evaluation of the topographic mapping accuracy using a second order polynomial function produced an RMSEz of +/-11 m, which theoretically would allow contouring at between 22 m, or twice the RMSEz, and 33 m interval, or 3 times the RMSEz. Manual contouring of the ASTER stereomodel revealed that while accurate landform shape could be produced, it is not precise enough to contour at 20 m interval. One should note again the impact of the tree canopies, making it difficult to contour on the ground surface. Tree canopies have also adversely affected the stereocorrelation because the DEM correlation was frequently on those canopies rather than on the ground surface. Subsequent work by Jordan et al. (2005) indicated that a planimetric accuracy (i.e. RMSExy) of ±10.3 m was achievable.

In conclusion, this research has confirmed that VNIR imagery can be employed to classify land use/cover at Anderson's Level I scheme, and with the use of an unsupervised approach, Level II can be achieved. The ASTER VNIR imagery's higher spatial resolution requires an object-based unsupervised rather than a per-pixel based supervised approach for image classification. In topographic mapping, ASTER bands 3N and 3B produced stereomodels that can map a moderate relief area (100-300 m AMSL range) at scales of 1:50,000 and smaller.

References

Abrams, M., and Hook, S. (1995), "Simulated ASTER data for geologic studies." *IEEE Transactions on Geoscience and Remote Sensing*, 33**,** 692–699.

Abrams, M., Hook, S., and Ramachandran, B., (v. 2). *ASTER User Handbook (version 2),* Pasadena, CA, Jet Propulsion Laboratory and Sioux Falls, SC, EROS Data Center, http://asterweb.jpl.nasa.gov/documents/aster_user_guide_v2.pdf Last accessed, 12-23-2003.

Anderson, J. R., Hardy, E. E., Roach J.T., and Witmer, R. E. (1976), "A land use and land cover classification system for use with remote sensor data." Geological Survey Professional Paper 964, Washington D.C., *United States Department of the Interior*, United States Government Printing Office

Aniello, P. (2003), "Using ASTER DEMs to produce IKONOS orthophotos." Proceedings: Fall Conference, *American Society for Photogrammetry and Remote Sensing*, Charleston, SC, October 2003.

Bischof, H., Schneider, W., & Pinz, A.J. (1992), "Multispectral classification of Landsat-images using neural networks. *IEEE Transactions on Geoscience and Remote Sensing*, 30:3, pp. 482-490.

Bjorgo, E. (2000), "Using very high spatial resolution multispectral satellite sensor imagery to monitor refugee camps." *International Journal of Remote Sensing,* 21:3, pp. 611-616.

Bolch, T. (2004), "Using ASTER and SRTM DEMs for studying glaciers and rock glaciers in northern Tien Shan." Proceedings: Part I, *Theoretical and applied problems of geography on a boundary of centuries*, Almaty, Kasakhstan, June 2004, p. 254-258. http://www.geographie.uni-erlangen.de/tbolch/lit/Bolch_almaty04.pdf Last accessed, 4/6/06.

Buchroithner, M.F., Kaufmann, V., Mansberger, R. (1987), "Austrian results of the LFC OEEPE test on map compilation and revision for developing countries." Proceedings; International Science Colloquium on the Use of

Bureau of the Census (2000). *Census 2000*, Washington, D.C. http://factfinder.census.gov/servlet/GCTTable?ds_name=DEC_2000_SF1_U&geo_id=04000US13&_box_head_nbr=GCT-PH1&format=ST-2 Last accessed, 1-7-04.

Büyüksalih, G., Kocak, M.G., Oruc, M., Akcin, H., Jacobsen, K. (2003). "Accuracy analysis, DEM generation and validation using Russian TK-350 stereo-images." *Photogrammetric Record*, 19:107, p. 200, http://www.blackwell-synergy.com/links/doi/10.1111/j.0031-868X.2004.00279.x/abs/

Büyüksalih, G. & Jacobsen, K (2004), "Generation and validation of high resolution space DEMs." Proceedings: Annual Conference, *American Society for Photogrammetry and Remote Sensing*, Denver, CO, May 2004.

Chauhan, N.S., Miller S., Ardanuy, P., (2003), "Spaceborne soil moisture estimation at high resolution: A microwave-optical/IR synergistic approach." *International Journal of Remote Sensing,* 24:22, pp. 4599-4622.

Chen, L.C., Teo, T.A. (2002), "Rigorous generation of digital orthophotos from EROS 1 high resolution satellite images." *International Archives of Photogrammetry and Remote Sensing*, 34:B4, Ottawa, pp. 620-625.

Cheng, F., & Thiel, K.H. (1995), "Delimiting the building heights in a city from the shadow in a panchromatic image - Part 1: test of 42 buildings." *International Journal of Remote Sensing*, vol. 16, pp. 409-415.

Cheng, X., Zhang, Y., Dongchen, E, Li, Z., Shao, Y. (2003), "Digital elevation model construction using ASTER stereo VNIR scene in Antarctic in-land ice sheet." Laboratory of Remote Sensing Information Sciences, Institute of Remote Sensing Applications, *Chinese Academy of Sciences*, Beijing, P.R.C..
http://lab.irsa.ac.cn/~xiaoxiao/paper/PID19840.pdf Last accessed 6/22/04

Chmiel, J., Kay, S., & Spruyt, P. (2004), "Orthorectification and geometric quality assessment of very high spatial resolution satellite imagery for common agricultural policy purposes." Proceedings, *XXth ISPRS Congress*, Istanbul, July, 2004.
http://www.isprs.org/istanbul2004/comm4/papers/492.pdf Last accessed, 2/18/06

CNES (2003a), "Spot Products and Services Price List." *Centre National d'Etudes Spatiales*.
http://www.spotimage.fr/automne_modules_files/standard/public/p336_ba582c667a21f3b7d1108ad9773629fdListe-de-Prix-anglais.pdf
Last accessed, 4/2/06

CNES (2003b), "Spot Satellite Technical Data." *Centre National d'Etudes Spatiales*.
http://www.spotimage.fr/automne_modules_files/standard/public/p229_fileLINKEDFILE_satp_en.pdf
Last accessed, 8/4/04

Comber, A.J., Law, A.N.R., Lishman, J.R. (2004), "Application of knowledge for automated land cover change monitoring." *International Journal of Remote Sensing*, 25:16, pp. 3177-3192.

Congalton, R., Oderwalk, R. & Mead, R. (1983), "Assessing Landsat classification accuracy using discrete multivariate analysis statistical techniques." *Photogrammetric Engineering and Remote Sensing*, 49:12, pp. 1671-1678.

Congalton, R. (1988), "Using spatial autocorrelation analysis to explore the errors in maps generated from remotely sensed data." *Photogrammetric Engineering and Remote Sensing*, 54:5, pp. 587-592.

De Cola, L. (1989), "Fractal analysis of a classified Landsat scene." *Photogrammetric Engineering and Remote Sensing*, 55:5, pp. 601-610.

DARA (2003), "MOMS-02." Web page, *German Space Agency*:
http://www.nz.dlr.de/moms2p/techdat/ Last accessed 8/4/04

Dowman, I.J. and Peacegood, G. (1989), "Information content of high resolution satellite imagery." *Photogrammetria*, vol. 43, pp. 295-310.

Dowman, I. J. (1994), "Satellite imagery - a guide to mapping applications." *Geomatics World*, 2:3.

Dowman, I.J. and Michalis, P. (2003), "Generic rigorous model for along track stereo satellite sensors. Proceedings: Joint ISPRS / EARSeL Workshop [International Society for Photogrammetry and Remote Sensing / European Association of Remote Sensing Laboratories]: High Resolution Mapping from Space 2003, *Institute of Photogrammetry and GeoInformation*, University of Hannover, Germany.

Doyle, F. (1979), "A large format camera for Shuttle." *Photogrammetric Engineering and Remote Sensing*, vol. 45, pp. 73-78.

Ehlers, M., and Welch, R. (1987), "Stereo-correlation of Landsat-TM images." *Photogrammetric Engineering and Remote Sensing*, vol. 53, pp. 1231-1237.

Ehlers, M., Gähler, M., and Janowski, R. (2003), "Automated analysis of ultra high resolution remote sensing data for biotope type mapping: New possibilities and challenges." *ISPRS Journal of Photogrammetry & Remote Sensing*, 57:5/6, pp. 315-326.

Foody, G. M. (2002), "Status of land cover classification accuracy assessment." *Remote Sensing of Environment*. 80:1, pp. 185-203.

Giri, C., Defourny, P., Shrestha, S. (2003), "Land cover characterization and mapping of continental Southeast Asia using multi-resolution satellite sensor data." *International Journal of Remote Sensing*, 24:21, pp. 4181-4196.

Graff, L.H. & Usery, E.L. (1993), "Automated classification of generic terrain features in digital elevation models." *Photogrammetric Engineering and Remote Sensing*, 59:9, pp. 1409-1417.

Gugan, D. J. & Dowman, I. J. (1988), "Topographic mapping from SPOT imagery." *Photogrammetric Engineering and Remote Sensing*, 54:10, pp. 1409-1414.

Gruen, A. & Speiss, E. (1986), "Point positioning and mapping with Large Format Camera data." ESA Proceedings; *International Geoscience and Remote Sensing Symposium on Remote Sensing: Today's Solutions for Tomorrow's Information Needs*, vol. 3, pp. 1485-1494.

Hirano, A., Welch, R., Lang, H. (2003), "Mapping from ASTER stereo image data: DEM validation and accuracy assessment." *Journal of Photogrammetry and Remote Sensing*, International Society for Photogrammetry and Remote Sensing, vol. 57, pp. 356-370.

Hord, R.M. & Brooner, W. (1976), "Land-use map accuracy criteria." *Photogrammetric Engineering and Remote Sensing*, 48:8, pp. 1299-1307.

Hurtt, G., Xiao, X.M., Keller, M., Palace, M., Asner, G.P., Braswell, R, Brondizio, E.S., Cardoso, M., Carvalho, C.J.R., Fearon, M.G., Guild, L., Hagen, S., Hetrick, S., Moore, B., Nobre, C., Read, J.M., Sa, T., Schloss, A., Vourlitis, G., Wickel, A.J. (2003), "IKONOS imagery for the Large Scale Biosphere-Atmosphere Experiment in Amazonia (LBA)." *Remote Sensing of Environment,* 88:1-2, pp. 111-127.

IEEE (2003), Forward to the special issue on urban remote sensing by satellite. *IEEE Transactions on Geoscience & Remote Sensing*, 41:9, pp. 1903-1906.

Jacobsen K. (1998), "Status and tendency of sensors for mapping." Web published: http://www.ipi.uni-hannover.de/html/publikationen/1998/jacobsen/jac_98_status_sm.pdf Last accessed 4/6/06

Jacobsen K. (2003), "DEM generation from satellite data." EARSeL Symposium, Ghent, 2003, *Remote Sensing in Transition*, Millpress, ISBN 90-77017-71-2, pp. 273-276.

Jacobsen, K. (2005), "High resolution satellite imaging systems, overview." Proceedings, ISPRS Workshop: *High Resolution Earth Imaging for Geospatial Information*, Hannover, May, 2005. http://www.ipi.uni-hannover.de/html/publikationen/2005/workshop/038-jacobsen.pdf Last Accessed, 2/18/06.

Jansen, L.J.M. and Gregorio, A. D. (2002), "Parametric land cover and land-use classifications as tools for environmental change detection." *Agriculture, Ecosystems & Environment*, 91:1-3, pp. 89-100.

JAXA (2003a), "Earth Observation Satellite: JERS 1, Optical Sensor - OPS." Web site, Earth Observation Research Center, National Space Development Agency of Japan*, Japanese Aerospace Exploration Agency*. http://www.eoc.nasda.go.jp/satellite/sendata/ops_e.html Last accessed 8/4/04

Jensen, J. R. (2000), "*Remote Sensing of the Environment: An Earth Resource Perspective*." Upper Saddle River, N.J., Prentice Hall.

Jordan, T.R., Lund, L.D., Lo, C.P. (2005), "Topographic mapping potentials of ASTER VNIR data." Proceedings: Annual Conference, *American Society for Photogrammetry and Remote Sensing*, Baltimore, Maryland, March 2005.

Kääb, A., Huggel., F., Wessels, R., Raup, B., Keiffer, H., Kargel, J. (2002), "Glacier monitoring from ASTER imagery: accuracy and applications." Proceedings: EARSeL / LISSIG Workshop [European Association of Remote Sensing Laboratories / Special Interest Group Land Ice and Snow]: *Observing Our Cryosphere from Space*, Bern, March 11-13, 2002.

Kaczynski, R. (1995), High resolution Russian satellite images for urban mapping. Proceedings; *GIS Special Group Meeting on Urban Applications*, Strasbourg, France.

Kamp, U., Bolch, T., Olsenholler, J. (2003), "DEM generation from ASTER satellite data for geomorphometric analysis of Cerro Sillajhuay, Chile/Bolivia." Proceedings: Annual Conference, *American Society for Photogrammetry and Remote Sensing*, Anchorage, Alaska, May 2003.

Kaufinan. YJ.. D.D. Herring, K.J. Ranson, and G.J. Gollatz (1998), "Earth Observing System AMI Mission to Earth, *IEEE Transactions on. Geoscience and Remote Sensing*, 36, pp. 1045-1055..

Kim, J.R. and Muller, J.P. (2002), "3D reconstruction from very high resolution satellite stereo and its application to object identification." *Proceedings: ISPRS Symposium on Geospatial Theory, Processing and Applications,* Ottawa, July 2002.
http://www.isprs.org/commission4/proceedings/pdfpapers/420.pdf Last accessed, 8/4/04

Konecny, G. & Schiewe, J. (1996), "Mapping from digital satellite image data with special reference to MOMS-02." *ISPRS Journal of Photogrammetry & Remote Sensing*, vol. 51, pp 173-181.

Murai, S. (1986), "Cartographic accuracy of stereo space photographs taken by large format camera: A case study in Japan." Proceedings; *ISPRS Symposium Mapping from Modern Imagery*, Edinburgh, Scotland, (Edinburgh, Scotland: Remote Sensing Society/ISPRS), Vol. 26, pp. 732-737.

Light, D.L. (1990), "Characteristics of remote sensors for mapping and earth science applications." *Photogrammetric Engineering & Remote Sensing*, 56:12, pp. 1613-1523.

Liu, W., Gopal, S., & Woodcock, C. (2004), "Uncertainty and confidence in land cover classification using a hybrid classifier approach." *Photogrammetric Engineering and Remote Sensing*, 70:8, pp. 963-971.

Lo, C.P. & Noble, E (1990), "Detailed urban land-use and land-cover mapping using large format camera photographs: An evaluation." *Photogrammetric Engineering and Remote Sensing*, 56:2, pp. 197-206.

Lo, C.P. and Yeung, A.W. (2002), *Concepts and Techniques of Geographic Information Systems.* Upper Saddle River, New Jersey, Prentice Hall, p. 116.

Lo, C.P. & Choi, J. (2004), "A hybrid approach to urban land use/cover mapping using Landsat 7 Enhanced Thematic Mapper Plus (ETM+) images." *International Journal of Remote Sensing*, 25:14, pp. 2687-2700.

Ma, F. (2004), "A comparison study on SPOT5 and ASTER sensor modeling." Proceedings: Annual Conference, *American Society for Photogrammetry and Remote Sensing*, Denver, CO, May, 2004.

Ma, Z. & Redmond, R.L. (1995), "Tau coefficients for accuracy assessment of classification of remotely sensed data. *Photogrammetric Engineering and Remote Sensing*, 61:4, pp. 435-439.

Maune, D.F., Huff, L.C., Guenther, G.C., (2001), "DEM User Applications." In Maune, D.F. *ed.*, *Digital Elevation Model Technologies and Applications: The DEM Users Manual,* Bethesda, MD, American Society for Photogrammetry and Remote Sensing, p. 368.

Microsystems, Inc. (2004), Web site, "*Satellite Industry Links.*"
http://www.satellite-links.co.uk/links/satop.html Last accessed, 8/12/04.

Moller-Jensen, L. (1990), "Knowledge-based classification of an urban area using texture and context information in Landsat-TM imagery. *Photogrammetric Engineering and Remote Sensing*, 56:6, pp. 899-904.

Mondello, C., Hepner, G.F., Williamson, R.A. (2004), "10-year industry forecast: Phases I-III, Study documentation." *Photogrammetric Engineering & Remote Sensing*, 70:1, pp. 5-58.

Mott, R. K. (1975), "The use of satellite imagery for very small scale mapping." *Photogrammetric Record*, 8:458-475.

Mulawa, D. (2004), "On-orbit geometric calibration of the Orbview-3 high resolution imaging satellite." Proceedings; Annual Conference, *American Society for Photogrammetry and Remote Sensing*, Denver, CO, May, 2004.

Muller, F., Donnay, J.P., & Kaczynski, R., (1994), "Evaluation of high resolution Russian satellite photographs for map revision up to the scale of 1:25,000." Proceedings; Com. IV Symposium on mapping and GIS, *International Society for Photogrammetry and Remote Sensing*, Athens, GA, pp. 304-310.

Myint, S.W., Lam, N, and Tyler, J. (2002), "An evaluation of four different wavelet decomposition procedures for spatial feature discrimination in urban areas." *Transactions in GIS,* 6:4, p. 403.

NMAS (1947), National Map Accuracy Standards, Bureau of the Budget, *Office of Management and Budget*, Washington, D.C..
http://erg.usgs.gov/isb/pubs/factsheets/fs17199.html

NOAA (2004), *Earth Imaging Satellite Database*. Web site, National Environmental Satellite, Data, and Information Service, *National Oceanic and Atmospheric Administration*.
http://commavail.noaa.gov/controlcenter.cfm Last accessed, 8/16/04.

Noguchi, M., Fraser, C., Nakamura, T., Shimono, T. (2004), "Accuracy assessment of QuickBird stereo imagery." *Photogrammetric Record*, 19:106, pp. 128-137.

Odenyo, V. and Pettry, D. (1977), "Land-use mapping by machine processing of Landsat-1 data." *Photogrammetric Engineering and Remote Sensing*, 43:4, pp. 515-523.

Oruca, M., Marangoz, A. M., G. Buyuksalih (2004), "Comparison of pixel-based and object-oriented classification approaches using Landsat-7 ETM spectral bands." Proceedings: XXth ISPRS Congress, *International Society for Photogrammetry and Remote Sensing, Istanbul, Turkey, July 12-23.*

PE&RS (2004), "New Landsat Data Continuity Strategy Announced by the Executive Office of the President." *Photogrammetric Engineering and Remote Sensing*, 70:11, p1221.

Petrie, G. (1970), "Some considerations regarding mapping from earth satellites." *Photogrammetric Record*, 6:36, pp. 590-624.

Petrie, G. (1985), "Remote Sensing and topographic mapping," in Kennie, T.J.M. and Matthews, M.C. (eds), *Remote Sensing in Civil Engineering*, Surrey University Press, Glasgow, pp 119-11.

Radarsat International (2004), Overview webpage:
http://www.radarsat2.info/rs2_satellite/overview.asp Last accessed, 6/24/04

Ridley, H. M., Atkinson, P. M., Aplin, P., Muller, J.P., & Dowman, I. (1997), "Evaluation of the potential of the forthcoming US high-resolution satellite sensor imagery at the ordnance survey." *Photogrammetric Engineering and Remote Sensing*, vol. 63, pp. 997-1005.

Rodriguez, E., Morris, C.S., & Belz, J.E. (2006), "A global assessment of the SRTM performance." *Photogrammetric Engineering and Remote Sensing*, vol. 72:3, pp. 249-260.

Roth, A., Eineder, M., Schättler, B. (2003), "TerraSAR-X: A new perspective for applications requiring high resolution spaceborne SAR data." Proceedings; Joint ISPRS/EARSeL Workshop (International Society for Photogrammetry and Remote Sensing / European Association of Remote Sensing Laboratories): High Resolution Mapping from Space 2003, *Institute of Photogrammetry and GeoInformation*, University of Hannover, Germany.

Rowan, L. C., Mars, J. C. (2003), "Lithologic mapping in the mountain pass, California area using Advanced Spaceborne Thermal Emission and Reflection Radiometer (ASTER)." *Remote Sensing of Environment*, 84:3, pp. 350-366.

Sandau, R. (2003), "Small satellites: What are the prospects for topographic mapping in the next decade." Proceedings: Joint ISPRS/EARSeL Workshop (International Society for Photogrammetry and Remote Sensing / European Association of Remote Sensing Laboratories): High Resolution Mapping from Space 2003, *Institute of Photogrammetry and GeoInformation*, University of Hannover, Germany.

Sawaya, K.E., Olmanson, L.G., Heinert, N.J., Brezonik, P.L., Bauer, M.E, (2003), "Extending satellite remote sensing to local scales: Land and water resource monitoring using high-resolution imagery." *Remote Sensing of Environment*, 88:1-2, pp. 144-156.

Shi, W. and Shaker, A. (2003), "Analysis of terrain elevation effects on IKONOS imagery rectification accuracy by using non-rigorous models." *Photogrammetric Engineering and Remote Sensing*, 69:12, pp. 1359-66.

S.I.C. (2004), "*Sensor Systems for Worldwide Satellite Imagery*." Web site: Spatial Information Clearinghouse, James Madison University, Harrisburg, VA.
http://www.hdic.jmu.edu/sic/vendors/satellite.htm Last accessed, 8/17/04.

Simard, R. (1983), "Digital stereo-enhancement of Landsat-MSS data." Proceedings; *Seventeenth International Symposium on Remote Sensing of Environment*, Ann Arbor, MI, May 9-13, 1983, pp. 1275-1281.

Simard, R., and Slaney, R., (1986), "Digital terrain model and image integration for geologic interpretation." Proceedings: *Fifth Thematic Conference on Remote Sensing for Exploration Geology,* Reno, Nevada, September 29 - October 2. Publisher: Environmental Research Institute of Michigan, Ann Arbor, MI, pp. 49-60.

Simard, R. and Krishna, V. G. (1983), "A successful approach in three dimensional perception of stereo Landsat-MSS images over cordilleran relief." Proceedings; *9th International Symposium on Machine Processing of Remotely Sensed Data*, West Lafayette, Indiana, pp. 31-40.

Smits, P. C., Dellepiane, S. G., and Schowengerdt, R. A. (1999), Quality assessment of image classification algorithms for land-cover mapping: a review and a proposal for a cost-based approach. *International Journal of Remote Sensing*, 20:8, pp.1461-1486.

Stoney, W. E. (2005), "Guide To Land Imaging Satellites." American Society for Photogrammetry and Remote Sensing, http://www.asprs.org/news/satellites/ASPRS_DATABASE_020206.pdf Last accessed 2/18/06.

Subramanian, K.S.S., Singh, A., Sudhakar, M. (2003), "Evaluation of digital elevation models created from different satellite images." *RMSI, Ltd*., Noida, India.
http://www.rmsi.com/PDF/evaluation%20of%20digital%20elevation%20models%20created%20from%20different%20satellite%20images.pdf
Last accessed, 6/23/04

Togliatti, G. & Moriondo, A. (1986), "Large Format Camera: The second generation photogrammetric camera for space cartography." Proceedings; ESA/EARSeL (European Space Agency/European Association of Remote Sensing Laboratories): *Europe From Space Symposium*, pp. 15-18.

Toll, D.L. (1985), "Effect of Landsat Thematic Mapper sensor parameters on land cover classification. *Remote Sensing of Environment*, vol. 17, pp. 139-140.

Tolono, F.G. & Poli, D. (2003), "Georeferencing of EROS-A1 high resolution images with rigorous and rational function model." Proceedings; Joint ISPRS/EARSeL Workshop - High Resolution Mapping from Space 2003, *Institute of Photogrammetry and GeoInformation*, University of Hannover, Germany.

Toth, C., Berning, S., James, L., Grejner-Brzezinska, D. (2001), "Integration of lidar data with simultaneously acquired digital imagery." Proceedings; Annual Conference, *American Society for Photogrammetry and Remote Sensing*, St. Louis, MO.

Toutin, T. (2001a), "Elevation modeling from satellite visible and infrared (VIR) data." *International Journal of Remote Sensing*, 22:6, pp. 1097-1125.

Toutin, T. (2002b), "DEM from stereo Landsat 7 ETM+ data over high relief areas." *International Journal of Remote Sensing*, 23:10, pp 2133-2139.

Toutin, T. (2004a), "DTM generation from Ikonos in-track stereo images using a 3D physical model." *Photogrammetric Engineering and Remote Sensing*, 70:6, pp. 695-702.

Toutin, T. (2004b), "Geometric processing of remote sensing images: models, algorithms and methods." *International Jounal of Remote Sensing*, 25:10, pp. 1893-1924.

Townsend, J.R.G., & Justice, C.O. (1980), "Unsupervised classification of MSS Landsat data for mapping spatially complex vegetation." *International Journal of Remote Sensing*, vol. 1, pp. 105-120.

Trisakti, B. & Carolita, I. (no date), "Comparison result of DEM generated from ASTER Stereo Data and SRTM." *Indonesian National Institute of Aeronautic and Space* (*LAPAN*). Web published, G*ISDevelopment.net* http://www.gisdevelopment.net/technology/tm/tm001pf.htm Last accessed 4/5/06

University of Texas (2004), , Glossary of Cartographic Terms**,** Map Collection **,** *Perry-Castañeda Library*. http://www.lib.utexas.edu/maps/glossary.html Last accessed, 6/28/04.

Lins, K. (1994), "*Requirements Analysis Results.for Land Cover and Land Use Data*." Reston, VA, United States Geological Survey.

USGS (2005), ASTER Products Website; http://edc.usgs.gov/products/satellite/aster.html. Accessed 2-19-05.

Vignon, F., Arnaud, Y., Kaser, G. (2003), "Quantification of glacier volume change using topographic and ASTER DEMs: A case study in the Cordillera Blanca." Proceedings: IGARSS '03, Geoscience and Remote Sensing Symposium, *IEEE International*, Toulouse, France.

Van Genderen, J.L. and Lock, B.F. (1977), "Testing land-use map accuracy. *Photogrammetric Engineering and Remote Sensing*, vol. 43, pp. 1135-1141.

Wang, F. (1990), "Improving remote sensing image analysis through fuzzy information representation." *Photogrammetric Engineering and Remote Sensing*, 56:8, pp. 1163-1169.

Welch, R., & Lo, C. P. (1977), "Heights measurements from satellite images." *Photogrammetric Engineering and Remote Sensing*, vol. 43, pp. 1233-1241.

Welch, R. & Usery, E. L. (1984), "Cartographic accuracy of Landsat-4 MSS and TM image data." *IEEE Transactions on Geoscience and Remote Sensing*, 22:3.

Welch, R. (1989), "Desktop mapping with personal computers." *Photogrammetric Engineering and Remote Sensing*, 55:11, pp. 1651-1662.

Welch, R., Jordan, T., Lang, H., and Murakami, H. (1998), ASTER as a source for topographic data in the late 1990s*." IEEE Transactions on Geoscience & Remote Sensing*, vol. 36, pp. 1282-1289.

Wessels, R.L., Kargel, J. S., Kieffer, H. H. (2002), "ASTER measurement of supraglacial lakes in the Mount Everest region of the Himalaya." *Annals of Glaciology*, vol. 34, pp. 399-408.

Wilson, P.A. (1997), "Rule-based classification of Water in Landsat MSS images using the variance filter." *Photogrammetric Engineering and Remote Sensing*, 63:5, pp. 485-491.

Wolf, P. & Dewitt, B. A. (2000), *Elements of Photogrammetry*. McGraw Hill, Boston, 3rd ed.

Yamaguchi, Y., Fujisada, H., Tsu, H., Sato, I., Watanabe, H., Kato, M., Kudoh, M., Kahle, A. B., & Pniel, M. (2001), "ASTER early image evaluation." *Advanced Space Research*, 28:1, pp 69-76.

Zhu, G. & Blumberg, D.G. (2002), "Classification using ASTER data and SVM algorithms: The case study of Beer Sheva, Israel." *Remote Sensing of Environment*, 80:2, pp. 233-240.